RICE UNIVERSITY

Optical Properties of Strongly Coupled Plasmon-Exciton Hybrid Nanostructures

by

Nche Tumasang Fofang

A THESIS SUBMITTED
IN PARTIAL FULFILLMENT OF THE
REQUIREMENTS FOR THE DEGREE

Doctor of Philosophy

APPROVED THESIS COMMITTEE:

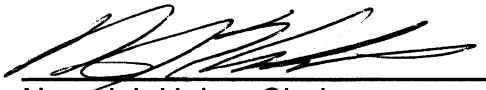

Naomi J. Halas, Chair
Stanley C. Moore Professor of Electrical and Computer Engineering
Professor of Chemistry

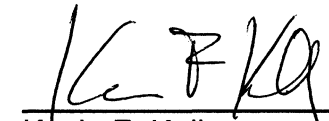

Kevin F. Kelly
Associate Professor of Electrical and Computer Engineering

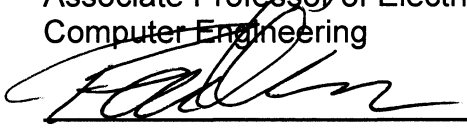

Peter J. Nordlander
Professor of Physics and Astronomy
Professor of Electrical and Computer Engineering

HOUSTON, TEXAS
November 2011

Abstract

Optical Properties of Strongly Coupled Plasmon-Exciton Hybrid Nanostructures

by

Nche Tumasang Fofang

Strongly coupled plasmon-exciton hybrid nanostructures are fabricated and their optical properties are studied. The plasmonic and excitonic systems are gold nanoshells and J-aggregates, respectively. Gold nanoshells are tunable plasmonic core-shell nanoparticles which can sustain distinct dipole and quadrupole plasmons with resonant energies dependent on core-size/shell-thickness ratio. J-aggregates are organic semiconducting material with excitons that possess very high oscillator strength making them suitable for coherent interaction with other kinds of excitations. The J-aggregates are formed on the surface of the nanoshells when a water/ethanol (50:50) solution of the dye molecules (2,2'-dimethyl-8-phenyl-5,6,5',6'-dibenzothiacarbocyanine chloride) is added to an aqueous solution of nanoshells. These nanoshell-J-aggregate complexes exhibit coherent coupling between localized plasmons of the nanoshell and excitons of the molecular J-aggregates. Coherent coupling strengths of 120 meV and 100 meV have been measured for dipole and quadrupole plasmon interactions with excitons, respectively. Femtosecond time-resolved transmission spectroscopy studies are carried out in order to understand the possible sources of optical nonlinearities in the nanoshell-J-

aggregate hybrid. Transient absorption of the interacting plasmon-exciton system is observed, in dramatic contrast to the photoinduced transmission of the pristine J-aggregate. An additional, transient Fano-shaped modulation within the Fano dip is also observable. The transient behavior of the J-aggregate-Au nanoshell complex is described by a combined one-exciton and two-exciton state model coupled to the nanoshell plasmon.

Acknowledgements

I am very grateful to my adviser, Prof. Naomi J. Halas, for creating a conducive research environment that promotes creativity and excellence. Her continuous support, guidance and encouragement have been invaluable to my progress through graduate school. I am indebted to all members of the Halas Group. A big thanks to Dr. Nathaniel Grady for always being available to help resolve ultrafast laser related problems; Britt Lassiter for his insightful questions that always propel me to go back and read some more; Dr. Bruce Brinson for introducing me to the world of optics alignment; Dr. Nikolay Mirin for his enthusiasm in assisting with any problem; Oara Neumann for always getting me extra SEM time and more; and, Jared Day for helping me forget about research through in-depth and insightful discussions about the general American culture. Thanks also to Dr. Rizia Bardhan, Dr. Surbhi Lal, Dr. Joseph Cole, Dr. Sri Priya Sundararajan, Dr. Janardan Kundu, Dr. Aoune Barhoumi, Mark Knight, Lisa Brown, Yu Zhang, Andie Schlather, Ciceron Ayala-Orozco, FangFang Wen, Nicholas King, Ryan Huschka, Shaunak Mukherjee and Christyn Thiboudeaux.

I will also like to thank Prof. Peter Nordlander, Prof. Alexander Govorov, Dr. Tae-Ho Park and Zhiyuan Fan for their theoretical input regarding my experimental results, and also, Prof. Kevin Kelly for accepting to serve on my PhD thesis defense committee.

My family has been of tremendous help, especially my parents: Pa Vincent Awah Fofang, Pa Titus Azeh Fofang, Pa Charles Fofang, Ma Lydia Fofang, Ma Martha Fofang and, Ma Cecilia Fofang. Pa Titus Azeh Fofang has been, and is still, a great source of inspiration. I am very grateful to Pa Titus Azeh Fofang for providing invaluable advise that has guided me through this PhD program, and also, for being very involved and engaged at every level of my project. I wish to thank my sister Lum Valerie and her husband Kenneth Mangong for their spiritual and financial support and also my sisters, Bih Jane Fofang and Gwendoline Azah Fofang for having my best interests at heart. Many thanks to my brother Nicholas Ndeh Fofang for his continuous guidance and also for always stopping in Houston to observe how grad school is treating me. Thanks to Peter Tumenta for his great enthusiasm and fascination of my research work. Thanks also to the following brothers and sisters, for without their prayers, success will not have been possible: Tamanjong Fru, Tangie Ngang, Bih Florence, Tsay Theodore, Vera Tuma, Anye Bernard (alias FC), Akwen Francisca, Yvonne Ngie, Mbeng Jacqueline, Dorothy Eyisab, Njie Wara, Afah Cho, Charles Fru, Ade Franklin, Che Julius, Bih Blanch, Iris Nchang, Dominic Ngante, Evelyn Ngante, Nchang Ngante, Che Emmanuel, Miranda Fofang, Eunice Fofang. Thanks also to the families of Dr. Chi Nche and Ma Tabitha Ayim.

Thanks to my friends Marx Mbonye, Joseph Young, Ben Appiah, Jeremy Neill, Uwana Ibanga, etc, etc, etc..... for the great times.

Table of Contents

List of Figures

Chapter 1

Introduction

1.1. Plasmonics

Plasmonics, commonly defined as optics at the nanoscale, has experienced tremendous growth in the last decade. This has been due to the numerous potential applications of plasmonics, and also the quest for a deeper understanding of the basics and fundamentals of plasmons. Plasmons are collective oscillations of conduction band electrons induced by electromagnetic excitation at their resonance frequency.[1] Basically, there are two types of plasmons: propagating surface plasmons and localized surface plasmons. Propagating surface plasmons are electromagnetic waves that propagate at the interface between a metal and a dielectric medium and coupled to the conduction band electrons of the metal. The field perpendicular to the direction of propagation decays evanescently into the dielectric layer. Localized surface plasmons (LSP) have no wave vector and they are sustained by metallic nanoparticles with sizes less than the excitation wavelength. The dimensions of these nanoparticles are comparable to or less than the electromagnetic skin depth,[2] thus, enabling the electromagnetic field to completely penetrate the metal perturbing the conduction band electrons.[3] The phase distribution of the field within the metallic structure is usually constant, giving rise to dipole charge distribution. For larger nanoparticles, phase retardation leads to the creation of higher order charge distributions within the nanoparticles resulting to quadrupole

plasmons, octupole plasmons, etc. The curved surface of the nanoparticle assists or enables the excitation of localized surface plasmons by exerting a restoring force on displaced electrons that subsequently results to resonance oscillations.[1] The work presented in this thesis involves only localized surface plasmons.

Enormous interest in the field of plasmonics stems from the fact that electromagnetic fields can be squeezed into domains with dimensions less than the diffraction limit, thereby giving rise to huge enhancements of the electromagnetic field intensity near the nanoparticle surface.[4, 5] Metallic nanoparticles sustaining LSP are analogous to optical cavities with a quality factor describing their resonance strength. The quality factors of metallic nanoparticles[6, 7] tend to be very small (10-100) [2] compared to those of optical cavities. This is due to the extreme short lifetime of LSP (a few tens of femto-seconds).[8] The short lifetime can be attributed to plasmon decay together with electron dephasing.[8] Dephasing results from elastic collision between electrons while decay can be both radiative and nonradiative. Radiative decay occurs when plasmons lose energy through the release of free space photons, while nonradiative decay is associated to energy lost through creation of electron-hole pairs (Landau damping).[8] For nanoparticles with sizes less than 100 nm, nonradiative decay tends to be dominant while radiative decay dominates for sizes greater than 100 nm. Metallic nanoparticles have a broad line-width[9] due to the short LSP lifetime and small quality factor, giving rise to a broad electron energy distribution within the plasmon. The LSP resonance wavelength depends

on the type of metal, shape, size and, dielectric environment. Advances in nanofabrication techniques have led to the realization of different kinds of nanoparticles, for example, nanorods,[10] nanorice,[11] nanoshells,[12] nanovoids,[13] nanodisks,[14] nanorings, fanoshells,[15] etc.

Based on the interesting properties of plasmons, possible areas of application include biomedicine,[16] chemical sensing,[17] energy harvesting,[18] information processing,[3, 19] etc. The optical absorption and scattering properties of metallic nanoparticles enable them to be used for diagnosing and ablating cancerous tumors.[20] The sensitivity of plasmon resonance wavelength to the dielectric medium makes metallic nanoparticles excellent chemical sensors.[21] The intense plasmonic near-field gives metallic nanoparticles the ability to function as SERS substrates,[5] and also, to be used for improving the efficiencies of both solar cells[18] and photo-thermal steam generation systems.

Different theoretical techniques have been developed to calculate the plasmonic modes of metallic nanoparticles. For nanoparticles with spherical and ellipsoidal symmetry, analytical solutions based on Mie and Gans theories are used.[22] When the nanoparticles have reduced symmetry, a numerical technique such as discrete dipole approximation (DDA), finite difference time domain (FDTD),[23] or finite element method (FEM) is employed. Plasmon hybridization[24] is applied for nanostructures with complex geometries, for example, nanomatryushka, fanoshells, nanoshells, plasmonic metamolecules (dimers, quadrumers, hexamers, heptamers), etc.

1.2. J-Aggregates

Research in plasmonics is being extended to study how plasmons interact with other kinds of excitations such as phonons[25] and excitons.[26] This effort is being driven by interest in active plasmonics [27, 28] where phonons or excitons are being used to control or manipulate properties of plasmons. The focus of this thesis is to study the linear[29] and nonlinear[30] optical properties of plasmon/exciton hybrid nanostructures.

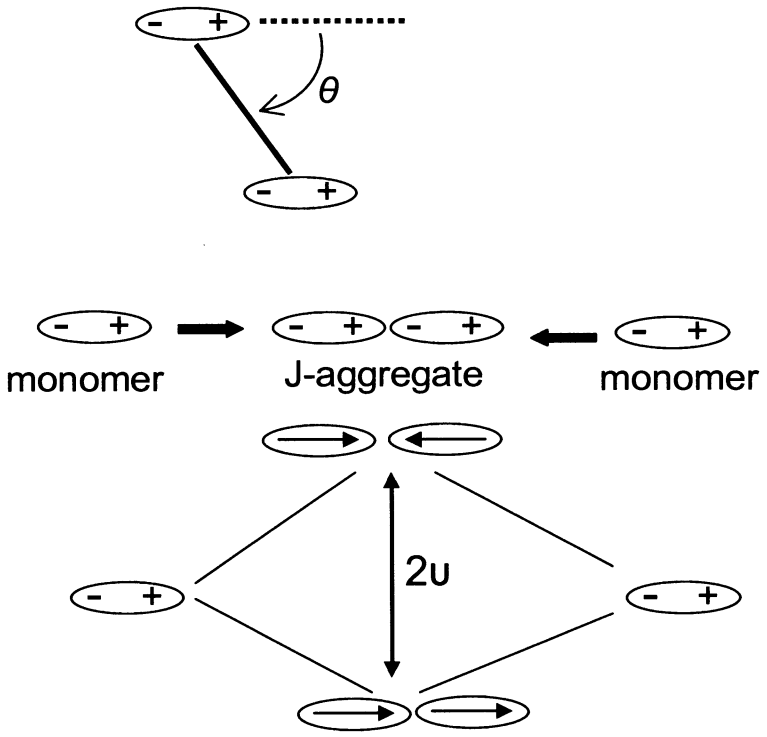

Fig. 1.1: Schematic illustration showing how interaction energy between monomers within an aggregate depends on monomer orientation. Hybridization of excited monomer states resulting to a low (bright) and high (dark) energy J-aggregate states.

The excitonic system used in this work consists of organic molecules that have the ability to form J-aggregates[31] in solution. A J-aggregate consists of a group of monomers which are aligned such that their dipole moment axis are parallel to each other (see Fig. 1.1 above). Within this group of monomers, excited states of different monomers hybridize or couple strongly with each other. Coupling energy depends on monomer orientation, distance between monomer dipoles and also the dipole moments. The coupling energy is given by:

$$U = \frac{|\mu|^2}{4\pi\varepsilon R^3}\left(1 - 3\cos^2\theta\right)$$

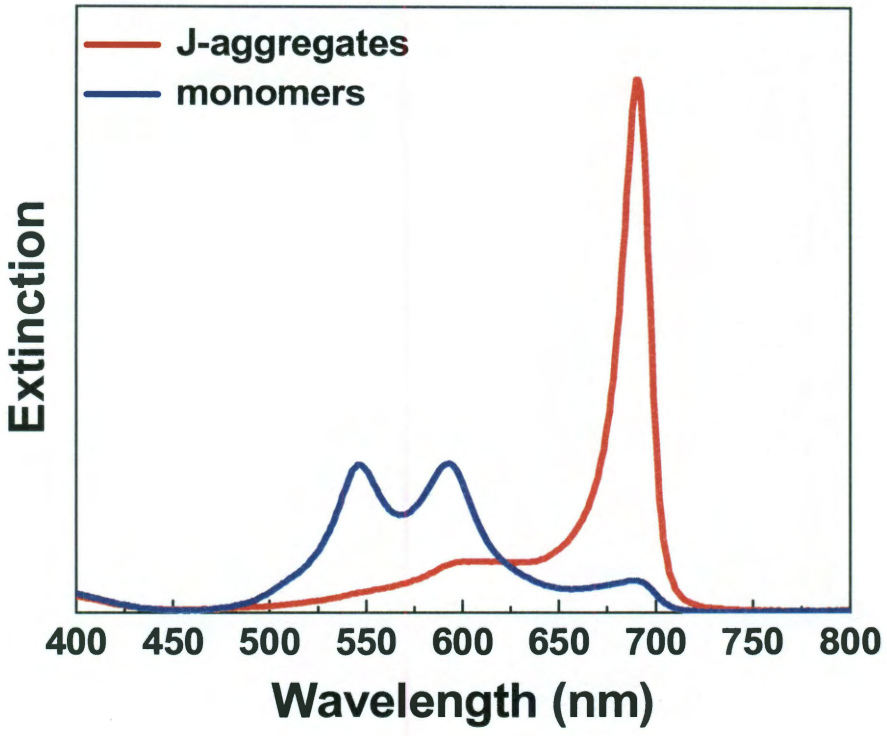

Fig. 1.2: Experimental absorption spectra of monomer molecules (blue) and their corresponding J-aggregate form (red). The J-aggregate spectrum is significantly red shifted and has a narrow line-width compared to the monomer spectrum. The organic moleculeused is 2,2'-dimethyl-8-phenyl-5,6,5',6'-dibenzothiacarbocyanine chloride.

As shown in Fig. 1.1 above, hybridization between excited monomer states results to the formation of low and high energy J-aggregate states. For the low energy J-aggregate state the transition dipole moments of the respective monomers oscillate in phase while for the high energy state they oscillate out of phase. Therefore, only the low energy J-aggregate state can be optically excited since it has a non-zero net dipole moment.[31] This explains why the experimental J-aggregate absorption spectrum is red shifted with respect to monomer absorption spectrum (Fig.1.2 above).

The absorption spectrum of the J-aggregates has a very narrow line-width compared to line-width of the organic molecule monomers. This narrow line-width is explained by the concept or notion of motional narrowing.[31] The narrow absorption line-width of J-aggregates implies the excitons of such a system have a very high oscillator strength[32-34] giving them the ability to interact strongly with other kinds of excitations. Another interesting property of J-aggregate is that they possess optically active two-exciton states with nonlinear properties.[33]

1.3. Fano Resonances and Plexcitons

The resonance line-width of localized surface plasmons is very broad when compared to that of excitons of J-aggregate. Therefore, an LSP/exciton hybrid can be viewed as an approximate representation of a system where a broad continuum excitation (LSP) interacts with a narrow discrete excitation (exciton).[35] Such a system is expected to exhibit Fano interference effects.[36] This is because the LSP can be excited through two different channels, that is,

excitation by incident electromagnetic radiation (Path 2 in Fig. 1.3) and by excited excitons of J-aggregates (Path 1 in Fig. 1.3). The excited exciton relaxes by transferring its energy to the plasmon through the Forster energy transfer process.[37] These two excitation channels show an energy dependent constructive and destructive interference effect referred to as the Fano resonances. The coulomb interaction between plasmons and excitons causes a modulation of plasmon properties, for example, a sharp decrease in scattering cross-section of plasmonic nanoparticle around the resonant exciton energy. On the part of the exciton, it experiences a red-shift in resonant excitation energy and probably energy level splitting.[38, 39] This implies there is a mixing between plasmons and excitons giving rise to a new hybrid excitation[35, 36] called plexcitons.[29, 30]

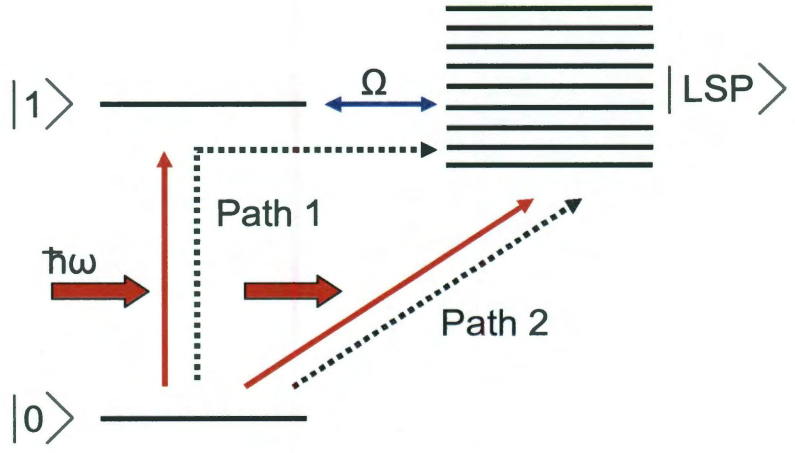

Fig.1.3: Energy level diagram showing the two paths through which localized surface plasmons (LSP) are excited. Destructive interference of these paths give rise to a Fano line-shape for a plasmon/exciton hybrid nanostructure.

The Fano resonance is a universal phenomenon which can be observed both in quantum[36] and classical systems.[40, 41] Recently, it was experimentally observed

between bright and dark plasmons in plasmonic nanostructures[15, 40, 42] and theoretically predicted to exist between excitons and plasmons of quantum_dot/metallic_nanoparticle hybrid nanostructure.[43] The linear[29] and nonlinear[30] optical properties of LSP/exciton hybrid structures presented in this thesis are Fano resonance effects.

1.4.0. Gold Nanoshells

In this work, I have used a kind of plasmonic nanostructure called the gold nanoshell[12] which consist of a dielectric silica core coated with a thin gold shell. For this project, the gold nanoshell has many advantages over other kinds of plasmonic nanostructures. For example, its LSP resonance wavelength can be easily tuned by varying the ratio of its core/shell radii.[21, 44] This tunability is very important because the resonance absorption energy of the exciton system (J-aggregate) is fixed. So, the gold nanoshell can be fabricated such that its LSP resonance wavelength overlaps the exciton absorption wavelength. Degeneracy in resonance energies of both plasmonic and excitonic systems is necessary in order for the two excitations to strongly interact with each other. Another interesting feature of the nanoshell is its intense near field.[5] In the plasmon/exciton hybrid structure, the J-aggregates form a shell around the gold nanoshell with the J-aggregates directly attached to the gold nanoshell surface.[26] Therefore the excitons are located directly within the intense electromagnetic field at the surface of the gold nanoshell. The interaction strength between plasmons and excitons increase with increase in intensity of the plasmonic fields.

Based on the gold nanoshell design, it can sustain distinct LSP modes which are unique and well defined. This makes it possible to study how excitons couple to different plasmonic modes as presented in this thesis.

1.4.1. Plasmon Hybridization Model

The tunability of the LSP resonance wavelength of gold nanoshell mentioned above can be explained on the basis of the plasmon hybridization model.[24] The plasmon hybridization model is a mesoscale electromagnetic analog of the molecular orbital theory used to predict how atomic orbitals interact to form molecular orbitals. The plasmon hybridization model separates complex particles into simpler subcomponents and calculates the interaction between the plasmons of these subcomponents. For a gold nanoshell, the plasmon hybridization model calculates the interaction between the plasmon sustained by a spherical gold particle (outer nanoshell surface) and a spherical gold cavity (inner nanoshell surface). Fig.1.4. shows a schematic of the plasmon hybridization of the particle and cavity plasmons to form symmetric and antisymmetric plasmon resonances of the gold nanoshell.

The tunability of nanoshells arises from the change in the strength of the interaction between the sphere and cavity plasmons as the thickness of the shell (interaction distance) changes.[45] For a thinner shell the interaction between the two plasmons increases leading to a greater splitting between the symmetric and anti-symmetric plasmon modes. Only the low energy symmetric mode can be optically excited, hence it is often referred to as the bright mode. The anti-

symmetric mode (dark mode) has a net dipole moment which is very small, and so, it cannot be optically excited.

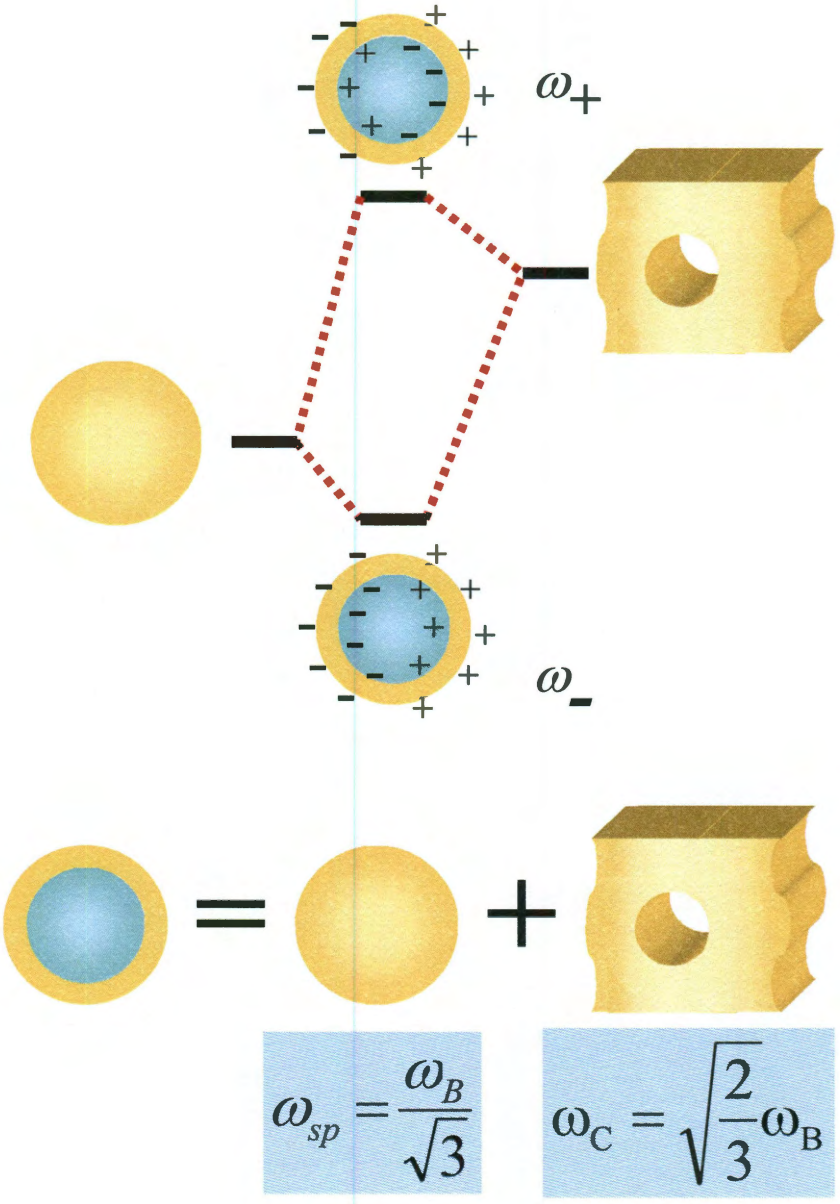

Fig. 1.4: Energy level diagram depicting plasmon hybridization in nanoshells resulting from interacting sphere and cavity plasmons. The two hybridized plasmon modes are an anti-symmetric plasmon resonance (ω+) and a symmetric plasmon resonance (ω-).

1.4.2. Gold Nanoshell Fabrication

The gold nanoshell fabrication technique is based on protocols previously developed and published.[12] The silica core is synthesized using the Stöber method of particle growth. Typically TEOS and ammonium hydroxide are mixed in varying ratios in ethanol to produce silica nanoparticles with the following diameters: 80 nm, 90 nm, 120 nm and 180 nm . After the silica particles are synthesized the surface is functionalized with 3-aminoproplytriethoxysilane (APTES). This chemical functionalization of the silica surface provides an amine moiety at the surface, which is used to attach small gold colloid. The small gold colloid particles 1-3 nm in size are synthesized by reducing chloroauric acid using tetrakis(hydroxymethyl)phosphonium chloride (THPC) as a reducing agent. The THPC-Au attached to the silica surface act as nucleation sites for the electrode-less deposition of Au to form a complete shell on the silica core. The electrode-less deposition was achieved by reducing gold from a solution of 1.8 mM potassium carbonate and 0.4 μM chloroauric acid by formaldehyde. The growth of a complete shell is monitored by UV-Visible spectroscopy.

1.5. Overview of the Work Presented in the Next Chapters

Chapter 2 presents the linear optical properties of Au nanoshell -J-aggregate hybrid nanostructures. Stable Au nanoshell-J-aggregate complexes are fabricated that exhibit coherent coupling between the localized plasmons of a nanoshell and the excitons of molecular J-aggregates adsorbed on its surface. By tuning the nanoshell plasmon energies across the exciton line of the J-

aggregate, plasmon-exciton coupling energies for these complexes are obtained. The strength of this interaction is dependent on the specific plasmon mode of the nanoparticle coupled to the J-aggregate exciton. From a model based on Gans theory, an expression for the plasmon-exciton hybridized states of the complex is obtained.

In chapter 3, ultrafast time-resolved transmission spectroscopy is used to study the nonlinear optical properties of the Au nanoshell-J-aggregate hybrid nanostructures. Time-resolved studies probe the dynamical behavior of the coupled system. Transient absorption of the interacting plasmon exciton system is observed, in dramatic contrast to the photoinduced transmission of the pristine J-aggregate. An additional, transient Fano-shaped modulation within the Fano dip is also observable. The behavior of the J-aggregate-Au nanoshell complex is described by a combined one-exciton and two-exciton model coupled to the nanoshell plasmons.

The possibility of achieving active plasmonic devices based on the principle of strong plasmon-exciton coupling is demonstrated in chapter 4. Strong plasmon-exciton coupling leads to system transparency at wavelength where plasmon and exciton energies are degenerate. Ultrafast all-optical modulation of this transparency is performed by modulating the ground state exciton population of J-aggregates in the gold-nanoshell/J-aggregate hybrid nanostructures. It is shown that devices functioning on this principle can operate at speeds much faster than 1THz.

The work is concluded in chapter 5 with suggestions of possible future research directions based on this thesis.

Chapter 2

Linear Optical Properties of Plexcitonic Nanoparticles

2.1. Introduction

Metallic nanoparticles in combination with molecular adsorbates provide one of the most adaptable architectures for the design and implementation of functionality at the nanoscale. For example, it has recently been shown that metallic nanoparticle - molecular adsorbate complexes can be designed that function as nanoscale pH meters,[46] light harvesters[47] and optically responsive, active nanocomplexes.[48] A prime reason for the broad utility of metallic nanoparticle-molecule complexes is the variety of mechanisms by which nanoparticle substrates and molecular adsorbates interact. For example, molecular adsorbates can modify the physical properties of nanoparticles by shifting their surface plasmon resonance,[49] or by imparting room temperature ferromagnetism to normally nonmagnetic nanoparticles.[50] Conversely, adsorbate properties such as fluorescence can be quenched or enhanced by the influence of a nanoparticle substrate,[51, 52] or Raman scattering cross sections of molecules can be greatly increased by appropriately designed nanoparticle substrates.[5, 17] Increased interactions between nanoparticles and molecular adsorbates should ultimately lead to strongly coupled complexes where the properties of both the nanoparticles and the adsorbates are mutually modified, resulting in new nanoparticle-based complexes with unique characteristics distinct from either the nanoparticle or molecular adsorbate properties alone.

Many of the interactions between metallic nanoparticles and molecular adsorbates are based on the collective electronic oscillations- localized surface plasmons- supported by metallic nanoparticles as a response to optical excitation at or near their resonant energies. Localized surface plasmons are spatially confined and have significantly enhanced fields at the nanoparticle surface relative to the incident excitation field. This enhanced near field can strongly modify the properties of molecules, molecular complexes, or other excitonic systems, within the fringing field of the nanoparticle. In the case of strong and coherent plasmon-exciton coupling, the properties of both the plasmon and the exciton are modified by their mutual interaction. To date, strong plasmon-exciton coupling has been observed in metallic films with propagating plasmons[53, 54] and in complex geometries where both propagating and localized plasmons both contribute to the overall interactions of the system.[13, 55] while coherent plasmon-exciton coupling has been observed between the fixed-frequency localized plasmons in Ag nanospheres and molecular J-aggregates.[56]

In this work, I report the formation of nanoshell-J-aggregate nanoparticle complexes that show coherent coupling (Fano Resonances) between the localized plasmons of the metallic nanoparticle and the excitons of the molecular J-aggregate. The plasmonic nanostructures used were Au nanoshells, tunable plasmonic nanoparticles consisting of a spherical silica core coated with a thin, uniform Au layer.[12] By varying the core size/shell thickness ratio, the plasmon energies of the nanoparticle can be systematically modified,[45, 57] and can be tuned through the exciton energy of the J-aggregate. This allows

for the direct measurement of the coupling energy of the nanoshell-J-aggregate complexes. In addition to varying the plasmon energy in this manner, increasing the nanoparticle size gives rise to additional multipolar plasmon modes.[44] Each spectrally distinct plasmon mode supports a unique angular and radial field distribution at the nanoparticle surface. In this series of experiments, two nanoshell size ranges were used, corresponding to the dipolar and the quadrupolar nanoshell plasmon mode, with the near field properties shown in Figure 2.1.

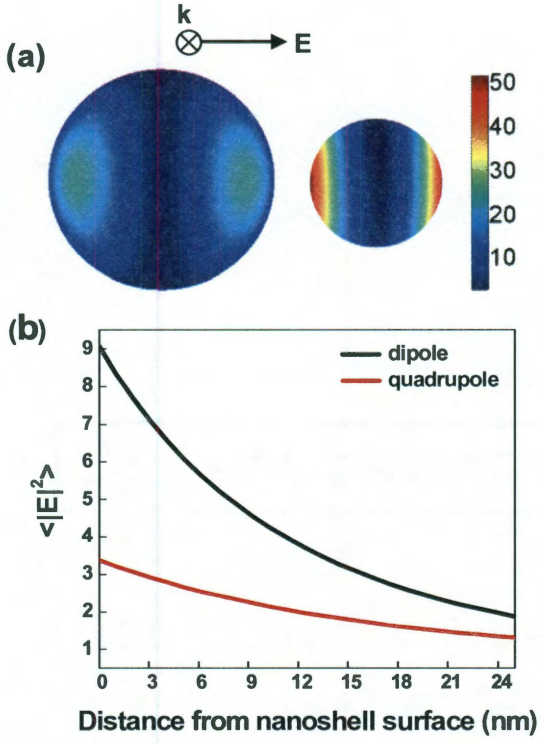

Figure 2.1: (a) Enhanced electromagnetic field intensity at the Au nanoshell surface corresponding at 693 nm excitation wavelength. The $[r_1, r_2]$ = [45, 63] nm nanoshell shows a distinct dipolar field which is more intense than the quadrupole field of the $[r_1, r_2]$ = [90, 120] nm nanoshell. **(b)** Variation of surface average field intensity ($\langle|E|^2\rangle$) with distance from nanoshell surface for nanoshells $[r_1, r_2]$ = [45, 63] nm and $[r_1, r_2]$ = [90, 120] nm.

Nanoshells with a core radius r_1 = 45 nm, resulting in a dipolar plasmon resonant with the J-aggregate exciton line; and nanoshells with a larger core radius r_1= 90 nm, with its quadrupolar plasmon resonant with the J-aggregate exciton, were designed and fabricated. In the nanoshell-J-aggregate complexes we report here, the strength of the plasmon-exciton coupling can be controlled by which specific plasmon mode of the nanoparticle couples to the excitonic J-aggregate. This simple and highly symmetric system provides an opportunity to theoretically analyze the plasmon-exciton coupling interaction in a quantitative manner. Using an analysis based on Gans theory, we obtain an analytical expression for the hybridized plasmon-exciton states of the system.

2.2. Fabrication of Plexcitonic Nanoparticles

The J-aggregate used in these experiments is formed from the dye 2, 2' dimethyl-8-phenyl 5, 6, - 5', 6' dibenzothiacarbocyanine chloride, a system having high oscillator strengths and narrow transition linewidths, suitable for achieving strong coupling at room temperature. The J-aggregate form of this dye has been well studied in coupling with other systems, such as cavity photons[58-61] and propagating plasmons.[53] A 0.5 mM solution of dye (2, 2' dimethyl-8-phenyl 5, 6, - 5', 6' dibenzothiacarbocyanine chloride[62]) in a mixture of water/ethanol (50/50 by volume) was used throughout the experiment (Fig. 2.2(a), inset). Addition of a polyvinyl alcohol solution transforms the dye to its J-aggregate form. Figure 2.2(a) shows extinction spectra of 3 μL of the dye solution in 3.5 mL of water (black) and aqueous polyvinyl alcohol (red). The J-aggregate form of this

dye has a narrow linewidth of nominally 20 nm and an absorption band that is redshifted to 693 nm[53] relative to the monomer peak absorbance at 547 nm. The peak at 593 nm (black) is due to J-aggregate formation in solution resulting from the presence of ethanol.

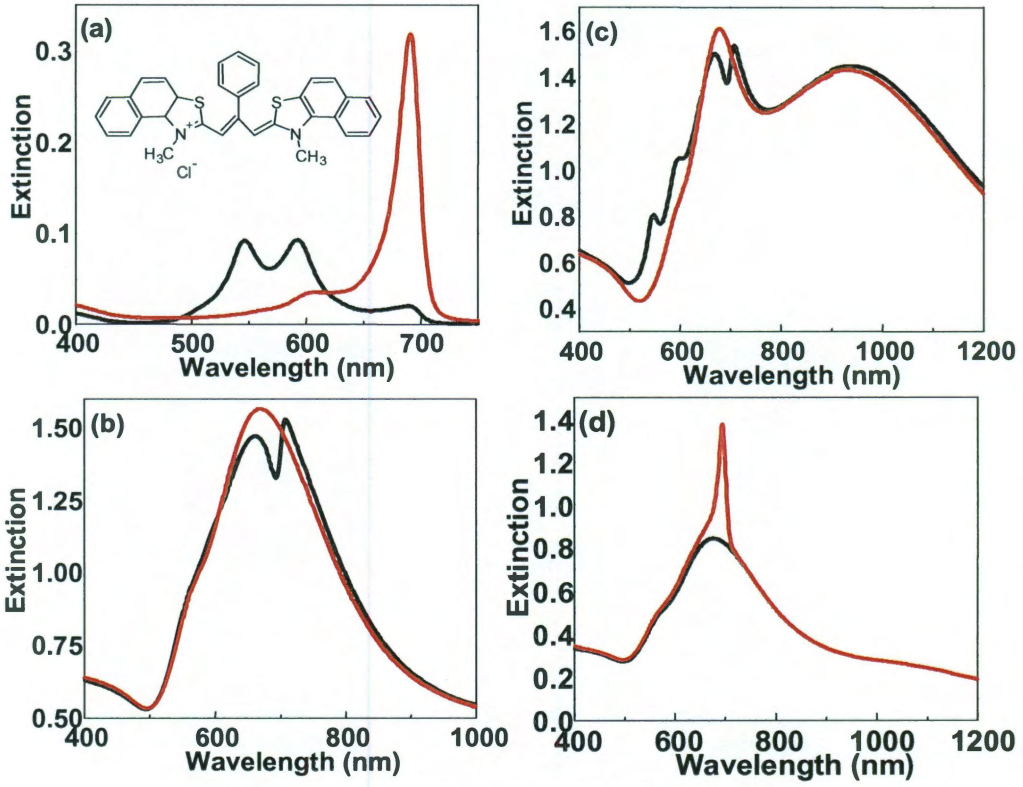

Figure 2.2: (a) Black: extinction spectrum of dye solution in 50/50 water/ethanol by volume. The peak at 547 nm is due to dye monomers while the peak at 593 nm results from aggregates induced by the presence of ethanol. **Red:** transformation of dye monomers to J-aggregates with absorption at 693 nm when 6 µl 0.5mM dye solution is added to 3.5 µl of aqueous polyvinyl alcohol. **Inset:** structure of the organic molecule 2,2'-dimethyl-8-phenyl-5,6,5',6'-dibenzothiacarbocyanine chloride. **(b) Red:** extinction spectrum of aqueous

solution of [r_1, r_2] = [45, 63] nm nanoshells with peak dipole plasmon resonance wavelength at 680 nm. **Black:** extinction spectrum of 3.5 ml of aqueous nanoshell solution to which 6 µl of 0.5 mM dye solution is added, revealing two hybrid peaks of almost equal intensity. **(c) Red**: extinction spectrum of aqueous solution of [r_1, r_2] = [90, 120] nm nanoshells with quadrupole plasmon resonance wavelength at 680 nm and dipole resonance at 950 nm. **Black:** 12 µl of dye solution is added to 3.5 µl of nanoshell solution results in two hybrid peaks. The peaks at 547 nm and 593 nm can be correlated to the peaks in black curve in **(a)**. **(d) Black:** extinction spectrum of nanoshell solution. Red: nanoshell and dye solution absorption in tandem cell.

Au nanoshells were fabricated as previously reported. Nanoshells are parameterized by the inner core and outer shell radii [r_1, r_2]. In Figure 2.2(b,c), the extinction spectra of [r_1, r_2] = [45, 63] nm nanoshells, and [r_1, r_2] = [90,120] nm nanoshells, respectively, are shown (red curves). The nanoshells are fabricated such that the dipole and quadrupole plasmon resonance energies are nearly degenerate with the J-aggregate absorption band. The [r_1, r_2] = [45, 63] nm nanoshells possess a strong dipole plasmon resonance at 680 nm and a weaker quadrupole plasmon resonance, seen as a small shoulder that appears at 570 nm. The [r_1, r_2] = [90,120] nm nanoshells have a strong quadrupole plasmon resonance at 680 nm along with a dipole plasmon at 950 nm.

The extinction spectra for nanoshells shown in Figure 2.2 (red curves) were obtained directly prior to the formation of the nanoshell-J-aggregate complex. To assemble the complexes, a volume of dye solution is added to an

aqueous solution in which Au nanoshells are suspended, and mixed well by shaking. The solution is then allowed to sit for at least 45 minutes, after which the extinction spectrum is measured. The resulting extinction spectra are shown in Figures 2.2(b,c) (black curves). The dipole and quadrupole plasmon peaks shown are strongly modulated by the presence of the J-aggregates, and have been transformed into two new peaks separated by a dip at 693 nm, which corresponds to the maximum absorption wavelength of the J-aggregate.

Several control experiments were performed to confirm the formation of the nanoshell-J-aggregate complex. In one experiment, separate solutions of nanoshells and J-aggregates were examined by UV-vis spectroscopy in a tandem cell (STARNA) where the beam path traverses the two separate solutions sequentially. J-aggregates were obtained as before, by mixing the dye solution with an aqueous polyvinyl alcohol solution, but not in the presence of nanoshells. The extinction spectrum from the tandem cell, shown in Figure 2.2(d), appears to be the direct addition of the nanoshell extinction spectrum and the J-aggregate dye extinction spectrum, quite distinct from the distorted lineshape observed in the plasmon linewidth of the nanoshell-J-aggregate complexes (Figures 2.2(b-c)). This experiment confirms quite definitively that the spectra shown in Figures 2.2(b) and (c) do not arise simply from the additive extinction of nanoshells and J-aggregates isolated from each other, but instead are directly the result of plasmon-exciton coupling.

The nanoshell-J-aggregate complexes appear to be formed through electrostatic self-assembly, due to the positively charged dye molecules and the

nanoshell surfaces that possess a net negative charge. It is quite possible that the J-aggregate complex formation in the presence of nanoshells may be initiated by this electrostatic attraction with the nanoshell surface. Following the mixing of nanoshells with dye solution, the peak transformation shown in Figure 2.2(b) and 2.2(c) from the red spectra to the black spectra progresses for 45 minutes, when it reaches its final, coupled state with no further changes in the extinction spectra. The resulting complexes appear to be remarkably stable: samples preserved for more than one month did not degrade. The weak spectral features that appear as shoulders at 547 nm and 593 nm in the extinction spectrum of the $[r_1, r_2]$ = [90, 120] nm quadrupolar nanoshell-J-aggregate complex (Fig. 2.2(c)- black curve) are attributable to residual dye monomers that remain in solution.

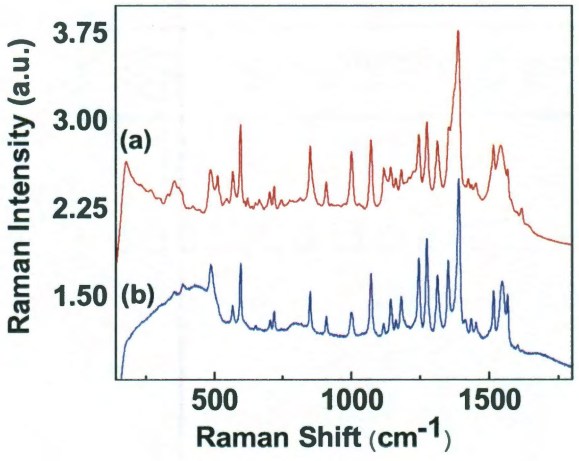

Figure 2.3: (a) SERS and (b) Normal Raman spectra of 2, 2'-dimthyl-8-phenyl-5, 6, 5', 6',-dibenzothiacarbocyanine chloride.

Surface enhanced Raman scattering (SERS) measurements were also performed to confirm the formation of the nanoshell-J-aggregate complex (Fig. 2.3). Nanoshells were first immobilized onto cleaned quartz substrates using a 0.1% by weight polyvinyl pyridine solution in ethanol, a procedure shown previously to yield well dispersed single nanoshells on a variety of substrate surfaces. Complex formation was performed by immersion of these nanoshell-coated quartz slides into 0.5mM dye solution for several hours. Before acquiring Raman spectra, the sample was rinsed several times with water. SERS spectra were obtained using a Renishaw inVia Raman microscope (Renishaw, United Kingdom) with 785 nm wavelength excitation, 55 μW laser power at the sample, a 63x water immersion lens (Leica, Germany) for light collection, and a 30 second integration time. Figure 2.3 shows the experimental (a) SERS spectra of the 2, 2'-dimethyl-8-phenyl-5, 6, 5', 6',-dibenzothiacarbocyanine chloride complexed with the nanoshells, compared with (b) normal Raman spectra of the same molecule in solution (normal Raman spectra of the isolated molecule and its J-aggregate in solution were found to be virtually indistinguishable). The strong SERS spectra directly confirm that the molecular J-aggregates remain bound to the nanoshell surface even after rinsing.

2.3. Results: Coherent Coupling between Plasmons and Excitons

In the nanoshell-J-aggregate complexes, the plasmons interact with excitons giving rise to plasmon/exciton mixed states. This process can be

described as a hybridization between the plasmons and excitons of the complex.[24, 63] Plasmon hybridization theory, which has been developed for the plasmon response of complex nanostructures,[24] can be extended to describe the interaction between nanoshell plasmons and J-aggregate excitons in this type of complex. In Figures 2.2(b) and (c), the peaks at low energy represent the bonding states (with the plasmonic and excitonic excitations in phase with each other) while those at high energy represent the anti-bonding states (when the plasmonic and excitonic excitations are out of phase). The fact that the two peaks in the spectra of Figures 2.2(b) and (c) are of almost equal intensity implies that the excitons and localized plasmons are in their strongest interaction regime. This is when the exciton resonance energy corresponds to the peak dipole or quadrupole plasmon resonance energy.

To determine the coherent coupling energy for the localized plasmon/exciton system, dispersion curves were obtained for the nanoshell-J-aggregate complexes. This was done by tuning the nanoshell plasmon resonance energy across the J-aggregate absorption band by varying the nanoshell core size /shell thickness (r_1/r_2) ratio. Nanoshells of dimensions [r_1, r_2] = [40, 58] nm, [40, 55] nm, [45, 63] nm, [45, 60] nm [45, 54] and [60, 83] nm were used to obtain data points for the dipole dispersion curve (Fig. 2.4) while [r_1, r_2] = [90, 127] nm, [90, 123] nm, [90, 120] nm, [90, 115] nm, [90, 110] nm and [90, 107] nm were used to obtain the data points for the quadrupole dispersion curve (Fig. 2.5). The order in which the nanoshell dimensions are listed corresponds to data points in each respective dispersion curve. The experimental extinction

spectra of the pristine nanoshells in water are shown in Figures 2.4(a) and 2.5(a), while those of the nanoshell-J-aggregate complexes are shown in Figures 2.4(c) and 2.5(c).

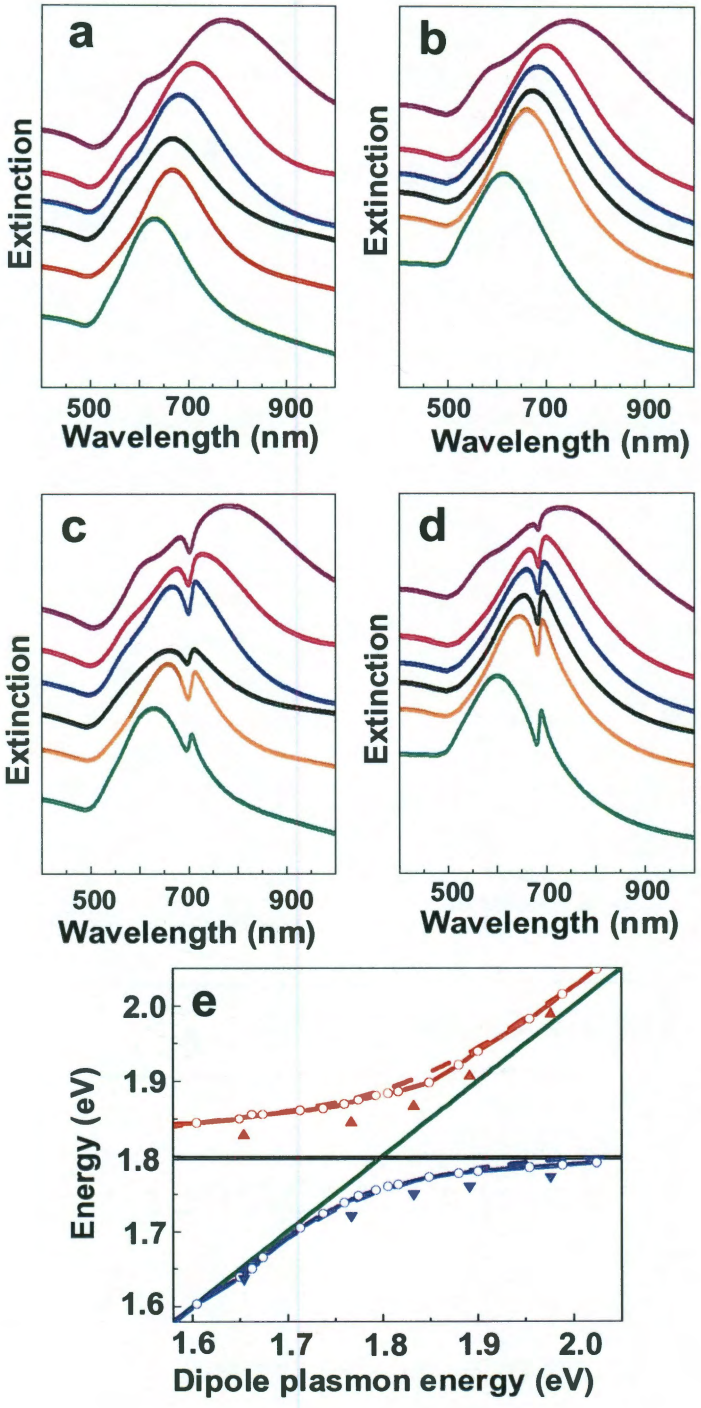

Figure 2.4: (a) Experimental extinction spectra of aqueous gold nanoshell solution showing dipole plasmon tuning. Nanoshell sizes from top to bottom are: $[r_1, r_2]$ = [60, 83] nm, [45, 54] nm, [45, 60] nm, [45, 63] nm, [40, 55] nm, [40, 58] nm. **(b)** Gold nanoshell extinction spectra obtained from Mie scattering theory. **(c)** Experimental extinction spectra of aqueous solution of gold nanoshell-J-aggregate complexes **(d)** Theoretical extinction spectra of gold nanoshell-J-aggregate complex obtained from Mie calculations. Johnson and Christy parameters are used for the Au shell and ε_1 =2.04 for the silica core. $\varepsilon_{\infty J}$ = 1, f = 0.02, and $\gamma \sim$ 0.052 for the J-aggregate molecular layer. **(e)** Dispersion curve from experimental data (diamond), Mie scattering theory (circle dashed line), and Gans theory (dashed line). The black and green lines represent uncoupled exciton and plasmon energies. Blue and red colors represent low and high energy plasmon-exciton hybrid states, respectively.

The number of nanoshells per ml of H_2O was approximately 6.68×10^9 for dipole samples and 1.86×10^9 for quadrupole samples. 12 µl of the dye solution was added to 3.5 ml of aqueous solution for each of the nanoshell solutions. Extinction spectra of all samples were obtained directly following the formation of the nanoshell-J-aggregate complexes. Peak energies of the resulting "plexcitonic" complexes were then plotted as a function of the plasmon energy of the pristine nanoparticles.

In the dispersion curves shown in Figures 2.4(e) and 2.5(e), the low energy plasmon/exciton peak is shown in blue and the high energy plasmon/exciton peak is shown in red. Uncoupled plasmon and exciton energies are represented by the green and black lines, respectively.

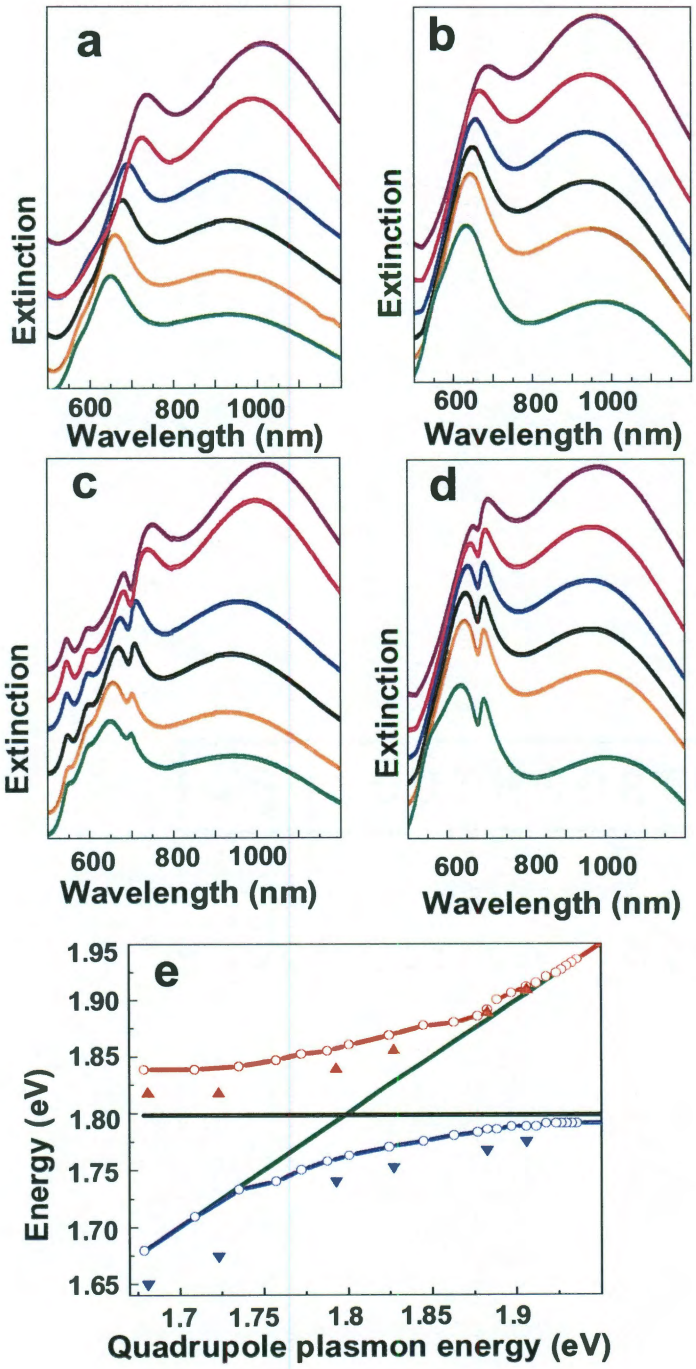

Figure 2.5: (a) Experimental extinction spectra of aqueous gold nanoshell solution showing quadrupole plasmon tuning. Nanoshell sizes from top to bottom are: $[r_1, r_2]$ = [90, 107] nm, [90, 110] nm, [90, 115] nm, [90, 120] nm, [90, 123] nm, [90, 127] nm. **(b)** Gold nanoshell extinction spectra obtained from Mie scattering theory. **(c)** Experimental extinction spectra of aqueous solution of gold nanoshell-J-aggregate complexes **(d)** Theoretical extinction spectra of gold nanoshell-J-aggregate complex obtained from Mie calculations. Johnson and Christy parameters are used for the Au shell and ε_1 =2.04 for the silica core. $\varepsilon_{\infty J}$ = 1, f = 0.02, and $\gamma \sim$ 0.052 for the J-aggregate molecular layer. **(e)** Dispersion curve from experimental data (diamond) and Mie scattering theory (circle dashed line). The black and green lines represent uncoupled exciton and plasmon energies. Blue and red colors represent low and high energy plasmon-exciton hybrid states, respectively.

The dispersion curves display an avoided crossing at the energy position where the uncoupled plasmon and exciton energies overlap. The splitting energy corresponds to the coupling strength between plasmons and excitons. The coupling energy from the dipole plasmon dispersion curve is approximately 120 meV while that from the quadrupole dispersion curve is less, approximately 100 meV.

2.4. Theoretical Model based on Gans Theory

To describe this system theoretically, we consider a concentric three layer model consisting of a two-layer spherical shell particle surrounded by a layer of J-aggregate (Fig. 2.6). ε_1 and ε_M are dielectric constants of the core (radius a) and background media, respectively; b denotes the radius of the nanoshell, and c denotes the radius of the nanoshell-J-aggregate complex. ε_2 is the dielectric constant of the Au shell layer with optical response given by the Johnson and Christy data[64] (used for the calculated extinction spectra) or the Drude model:

$$\varepsilon_2(\omega) = \varepsilon_\infty - \frac{\omega_p^2}{\omega^2 + i\Gamma\omega}$$

(1)

where ω is the frequency of the incident field, ω_p is the bulk plasmon frequency, Γ is the collision rate of electrons in Au, and ε_∞ is the high frequency component of the Au dielectric function. ε_3 is the dielectric constant of the J-aggregate molecule covering the Au nanoshell with optical response modeled by a Lorentzian absorption line shape:

$$\varepsilon_3(\omega) = \varepsilon_{\infty J} - f\frac{\omega_0^2}{\omega^2 - \omega_0^2 + i\gamma\omega}$$

(2)

where f is the reduced oscillator strength, γ is the line width, ω_0 is the transition frequency, and $\omega_{\infty J}$ is the high frequency component of the J-aggregate dielectric function.

First we calculate the optical spectra using Mie scattering theory, which consists of solving the vector wave equation of a time-harmonic electromagnetic field (E, H) derived from Maxwell equations.[65] To compare with experiment, we use the Johnson and Christy dielectric function data directly for the dielectric constant of the Au shell and ε_1 =2.04 for the silica core. For the J-aggregate, $\varepsilon_{\infty J}$ = 1, f = 0.02, and γ ~ 0.052 are used as the best parameters for fitting Eq. (2) to the absorption spectral lineshape. We chose ε_M = 1.77, corresponding to an aqueous medium. Figures 2.4(b) and 2.4(d) show results of Mie scattering theory for dipole nanoshells and nanoshell-J-aggregate complexes, while Figures 2.5(b) and 2.5(d) show the quadrupole nanoshell-based complex. Mie theory calculations accurately reproduce the experimental extinction spectra for both nanoshells and nanoshell-J-aggregate complexes. This implies that the coupling of plasmons and excitons can be microscopically understood in the classical electromagnetic context.

Next, we apply Gans theory to analyze the nanoshell-J-aggregate hybrid structure. Gans theory is a solution of Maxwell's Equations for plane wave excitation of a spheroidal metallic nanoparticle in the quasistatic approximation, taking into account only the dipolar component of the plasmon mode. The electric potential of the concentric two-layered spherical shell particle (Figure 2.6) in a uniform external electric field along an arbitrary direction is calculated by solving Laplace's equation with associated boundary conditions.

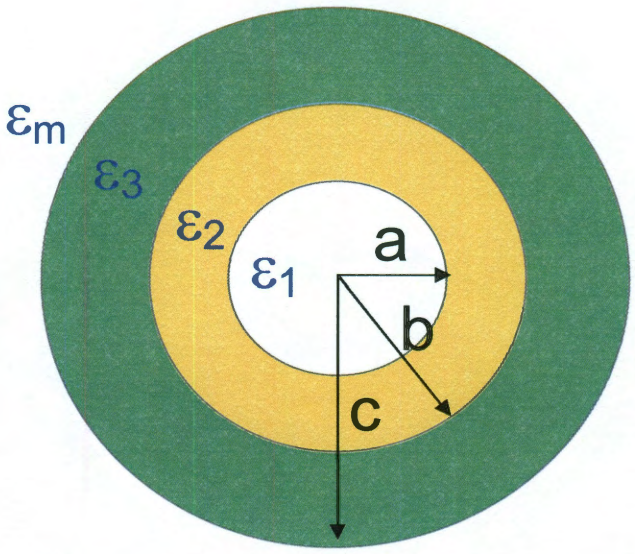

Figure 2.6: (a) Schematic description of gold nanoshell-J-aggregate complex model for theoretical calculation. $\varepsilon_1, \varepsilon_2, \varepsilon_3$ and ε_M represent silica core, gold shell, J-aggregate molecular layer and surrounding medium respectively. The core radius (a), nanoshell radius (b) and nanoshell-J-aggregate total radius of the complex (c) are shown.

Then the polarizability α of the system is obtained from the induced dipole moment divided by the external field.[66] This is expressed as:

$$\alpha = 4\pi\varepsilon_0 c^3 \frac{\varepsilon_{eff} - \varepsilon_M}{\varepsilon_{eff} + 2\varepsilon_M}$$

(3)

$$\varepsilon_{eff} = \varepsilon_3 \frac{A - 2\left(\frac{b}{c}\right)^3 B}{A + \left(\frac{b}{c}\right)^3 B}$$

(4)

$$A = (2\varepsilon_3 + \varepsilon_2)(2\varepsilon_2 + \varepsilon_1) + 2(\varepsilon_3 - \varepsilon_2)(\varepsilon_2 - \varepsilon_1)\left(\frac{a}{b}\right)^3$$

$$B = (\varepsilon_3 - \varepsilon_2)(2\varepsilon_2 + \varepsilon_1) + (\varepsilon_3 + 2\varepsilon_2)(\varepsilon_2 - \varepsilon_1)\left(\frac{a}{b}\right)^3$$

and ε_0 is the permittivity of free space.

The polarizability becomes frequency dependent after substituting the expressions for ε_2 and ε_3 from Eqs. 1 and 2 into Eq. 3. The optical absorption ($\sigma(\omega)$) is then calculated from the frequency dependent polarizability $\alpha(\omega)$ by the following formula:

$$\sigma(\omega) = \omega \mathrm{Im}[\alpha(\omega)]$$

(5)

For an analytical model, we use the following Drude parameters: $\varepsilon_\infty = 9.5$, $\omega_p = 9.0$ eV, $\Gamma = 0.5$ eV, for the Au shell. The new resonant modes ($\omega_{l-}^{\pm}$) are calculated from the equation $\frac{d\sigma(\omega)}{d\omega} = 0$ associated with Gans theory. These new resonant modes correspond to plasmon/exciton hybrid states resulting from the hybridization of the symmetric Au-nanoshell dipolar plasmon mode (ω_{l-}) and the resonant exciton mode (ω_0). As clearly shown on the dispersion curve (Fig. 2.4(e), Gans theory results are very similar to the results from experiment and from Mie scattering theory. Note that the theoretical dispersion curves are obtained in a similar manner as the experimental dispersion curves.

A simple analytical model for the coupling between the exciton and the plasmon can be derived by assuming that $\varepsilon_\infty = \varepsilon_M = \varepsilon_1 = 1$. In this limit, the tunable plasmon frequencies of Au nanoshells are:

$$\omega_{l\pm}^2 = \frac{\omega_p^2}{2}\left[1 \pm \frac{1}{2l+1}\sqrt{1+4l(l+1)\left(\frac{a}{b}\right)^{2l+1}}\right]$$

(6)

where l is the order of spherical harmonics with l = 1 representing the dipolar mode, l = 2 for the quadrupolar mode, l = 3 for the octupolar mode etc. The – (+) represents symmetric (antisymmetric) nanoshell plasmon mode. By varying the ratio $\frac{a}{b}$, the symmetric Au-nanoshell dipole plasmon mode ($\omega_{1-} = \frac{\omega_p}{\sqrt{2}}\left(1 - \frac{1}{3}\sqrt{1+8\left(\frac{a}{b}\right)^3}\right)^{1/2}$) is tuned across the resonant exciton transition mode (ω_0) as shown experimentally and theoretically in Figure 2.4(a) and 2.4(b). The interaction between ω_{1-} and ω_0 results in the formation of new modes (plasmon/exciton hybrid states) which we denote here by $\omega_{1-}^{\pm}$. The frequencies of these new states can be approximately obtained by equating the real part of the denominator of $\alpha(\omega)$ to zero and solving for the roots in the limit where Γ and γ approach zero. Using this method we obtain:

$$\left(\omega_{1-}^{\pm}\right)^2 = \frac{1}{2}\left(\omega_0^2(1+f) + \omega_{1-}^2\right) \pm \frac{1}{2}\sqrt{\left(\omega_0^2 - \omega_{1-}^2\right)^2 + \omega_0^4 D^2}$$

(7)

$$D^2 = f\left[(2+f)+\frac{2}{3}\left(1-4\left(\frac{b}{c}\right)^3\right)\frac{\omega_{1-}^2}{\omega_0^2}\right]$$

(8)

In the hybridization scheme D^2 can be regarded as a coupling term. We can generally interpret the coupling of Au-nanoshell plasmons and excitons from Eq. 8. The coupling strength increases as f and c increase, and does not change significantly for a very thick J-aggregate layer. On the other hand, the coupling strength decreases as f tends towards zero or as c approaches b. Therefore the magnitude of the splitting $\left|\omega_{1-}^{+}-\omega_{1-}^{-}\right|$ is controlled by the exciton oscillator strength and the thickness of the J-aggregate molecular layer.

2.5. Dependence of Coupling Strength on J-Aggregate Thickness

From our analysis it appears that the observed splitting energies for our nanoshell-J-aggregate complexes are limited by the thickness of the J-aggregate layer on the nanoparticle surface. Based on the molecular absorbance of the dye molecules and nanoshells used in this experiment, we estimate that the "effective" thickness, or the depth of J-aggregate coupled to the nanoshell plasmon, is nominally 4 nm. In an attempt to increase the splitting energy of the nanoshell-J-aggregate complex, nanoshells were first functionalized with sodium 2-mercaptoethanesulfonate prior to complexation with J-aggregates, to increase the negative charge on the nanoshell surface relative to complex formation with

pristine nanoshells. The pre-functionalized sulfonated nanoshells were then exposed to dye solutions of various concentrations to produce J-aggregates of various molecular coating thicknesses. The splitting energies of these complexes as a function of the dye concentration used in formation of the nanoshell-J-aggregate complexes are shown in Figure 2.7. While any further increase in splitting using this approach is rather small, indicating that the effective thickness may already have been reached, this experiment reveals a strong asymmetry in the onset of plasmon/exciton interaction in this complex, an effect that may be related to dielectric screening or phase retardation effects.[67]

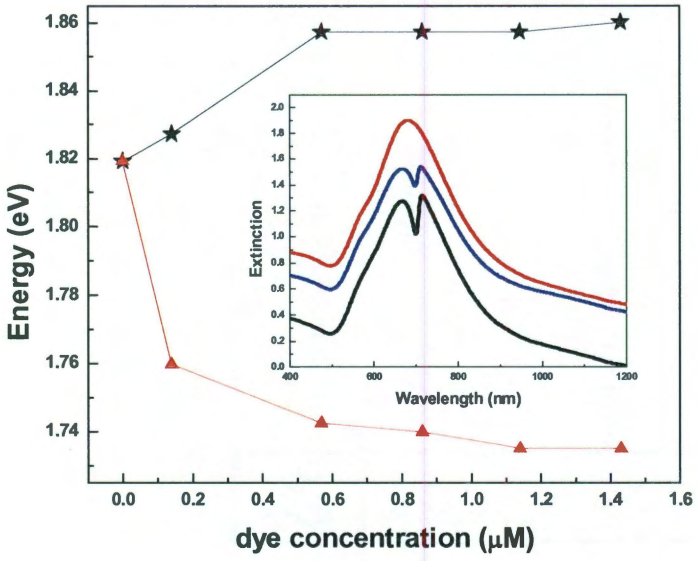

Figure 2.7. Onset of splitting in plasmon-J-aggregate complex as a function of dye concentration in media, which controls deposition of the J-aggregate adlayer on the nanoshell surface. Inset: nanoshell-J-aggregate plexciton spectra for various dye concentrations shown: 0 μL (red), 4 μL (blue), 10 μL (black). Spectra shown are offset for clarity.

2.6. Conclusions

In conclusion, we have fabricated nanoshell-J-aggregate complexes which manifest coherent coupling between the plasmons of the nanoparticle and the excitons of the J-aggregate complex. Strongly asymmetric splitting energies as large as 120 meV are observable in these complexes, where the splitting energy depends upon the plasmon mode of the complex. We believe that this result may stimulate interest in the fabrication and properties of coupled plasmon-exciton nanostructures with controlled coupling, and with optical properties unique to this new class of nanoparticle-based materials.

Chapter 3

Nonlinear Optical Properties of Plexcitonic Nanoparticles

3.1. Introduction

The optical nonlinearity of materials is a fundamental property required for the realization of active optical frequency devices such as ultrafast switches,[68-72] bistable devices,[73-76] limiters,[77] and modulators.[69, 78, 79] Most materials found in nature, however, have a very small nonlinear optical response. Fortunately, this response can be enhanced by exploiting the electronic or vibrational transitions in materials for resonant enhancement at the corresponding near-resonant energies.[80] This limitation can also be addressed by designing new, nanoengineered materials whose resonances are tuned to a frequency region of interest, such as specially designed plasmonic structures. Interactions with directly adjacent media can be enhanced by coupling within the intense evanescent field of the plasmon, resulting in new, nanocomposite hybrid materials whose properties are distinct from the properties of the individual constituent media.

Hybrid molecular-plasmonic nanostructures, where excitations of the respective components of the hybrid are designed to interact, provide a promising strategy for the development of active, nonlinear materials at optical frequencies.[43, 81] Ultrafast time-domain optical studies can reveal how these interactions result in new properties, and how processes like exciton-plasmon

hybridization, energy or charge transfer, may contribute to the new hybrid material response. Interest in the combination of molecular media and plasmonic nanostructures results from the ease in design and fabrication of hybrid media with these constituents, and also from the many opportunities to exploit the numerous interaction mechanisms associated with excitonic and plasmonic systems.

Metallic nanoparticles sustain collective electronic excitations, known as localized surface plasmons, when resonantly excited. The local electromagnetic field associated with these plasmons can be quite intense and well localized near the metallic nanoparticle surface; so much so that it may strongly modify the nonlinear properties of any material directly within this fringing field.[80] For example, the surface plasmon may affect absorption saturation, nonlinear absorption lineshapes,[81] nonlinear refractive index,[82] or nonradiative decay channels[83] in a directly adjacent medium, modifying the optical nonlinear response through any of these mechanisms.

This chapter reports the examination of the ultrafast optical dynamics of a hybrid resonant plasmon-exciton system consisting of a J-aggregate-Au nanoshell complex. Nanoshells are tunable plasmonic core-shell nanoparticles that support a distinct hierarchy of localized plasmon modes with resonant energies dependent on the relative dimensions and composition of their core and shell layers, the absolute size of the nanoparticle, and the presence of other media adjacent to, or surrounding, the nanostructure.[12, 48, 84] J-aggregates are organic semiconductors with localized excitations- excitons- that possess very

high oscillator strengths, suitable for interaction with the intense near field of localized surface plasmons.[29] Strong interaction of J-aggregate excitons with plasmons[53, 54] and cavity photons,[60, 61, 85] resulting in the formation of mixed states, have been reported. In these systems, the ultrafast dynamical properties of J-aggregates are strongly modified. Exciton-photon interactions have been extensively studied for J-aggregates in microcavities,[58, 86] and more recently for J-aggregates interacting with propagating surface plasmons on extended metallic structures.[87] Until now, however, the dynamical response of J-aggregate excitons due to coupling with the localized plasmons of plasmonic nanoparticles has not been directly examined. The ultrafast properties of metallic nanoparticle-J-aggregate complexes have been reported for the case where the transition energy of the J-aggregate is strongly detuned relative to the resonant plasmon energy;[56] however, this is a much weaker interaction regime which is substantially different from the stronger interactions in the doubly resonant regime addressed in the present study. In the weaker, nonresonant regime, the plasmon-molecule interaction typically leads to enhancement of molecular absorption and shifts in plasmon resonance frequencies. These characteristics are replaced by entirely new effects in the stronger interaction regime, where the coupled plasmons and excitons hybridize and form plexcitons, and where the behavior of this new highly coupled system is distinct from either of its component subsystems.[29] As has been recently shown in a number of plasmonic systems, strong coupling between metallic nanoparticles can lead to Fano interference and resonances.[15, 40-42, 88-91] Such interference can also occur in

metallic nanoparticle/semiconductor quantum dot hybrid systems where the coupling between excitons and plasmons can also result in an enhancement of the Fano effect.[81] Further increased coupling may lead to a transition from asymmetric Fano behavior to that of a doubly peaked Fano resonance, and finally to a bistable regime.[73] In the present study, we examine these interaction regimes experimentally for a hybrid J-aggregate-plasmonic nanostructure, and construct a straightforward nonlinear dielectric model that describes the observed interaction between the two subsystems.

3.2. Overview: Fabrication and Linear Optical Properties of Plexcitonic Nanoparticles

Our coupled plasmon-exciton nanocomplex consists of a nanoshell surrounded by an epilayer of J-aggregates (Fig. 3.1(a)). The J-aggregates are formed on the surface of the nanoshells when a water/ethanol (50:50) solution of the dye molecules (2,2'-dimethyl-8-phenyl-5,6,5',6'-dibenzothiacarbocyanine chloride) is added to an aqueous solution of nanoshells. With the peak of the nanoshell spectrum tuned to the maximum absorption of the J-aggregrate (Fig. 3.1(b)), the complexes exhibit coherent coupling between the localized plasmons of the nanoshell and excitons of the molecular J-aggregates: a well-defined Fano resonance is observed in the ensemble optical spectrum (Fig. 3.1(c)). The Fano resonance created well-expressed dips in the absorption spectra (~10%) and the corresponding spectral peak-to-peak distances were measured as ~ 100meV.[29] The Fano dip structure (anti-resonance) can be understood as a coherent destructive coupling between

two oscillations, an exciton and a plasmon. This coupling can be adequately described in terms of a classical dielectric model.[29]

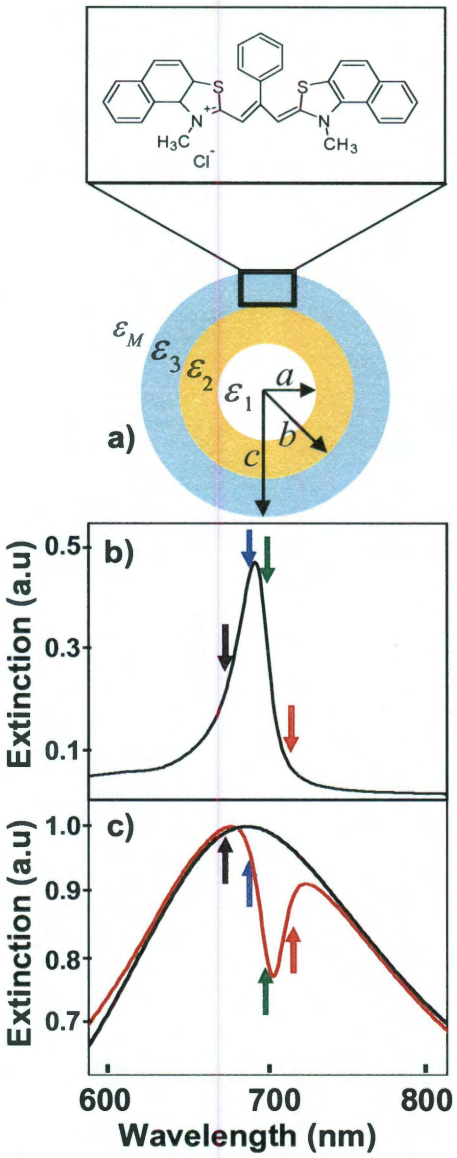

Figure 3.1: (a) Schematic of the hybrid nanocomplex consisting of a gold nanoshell coated with J-aggregate molecular film (2,2'-dimethyl-8-phenyl-5,6,5'6'-dibenzothiacarbocyanine chloride) **(b)** Extinction spectrum of the J-aggregate, obtained from a formulation consisting of a mixture of 6 □L of 117 □M dye solution and 3.5 mL of aqueous polyvinyl alcohol.**(c)** Extinction spectra of pristine (black) and J-aggregate coated (red) [r_1, r_2]=[41, 54] nm nanoshells. The vertical arrows indicate the wavelengths (680 nm, 690 nm, 700 nm, 710 nm) where the J-aggregates and J-aggregate coated nanoshells were optically interrogated.

3.3. Experimental Set-up

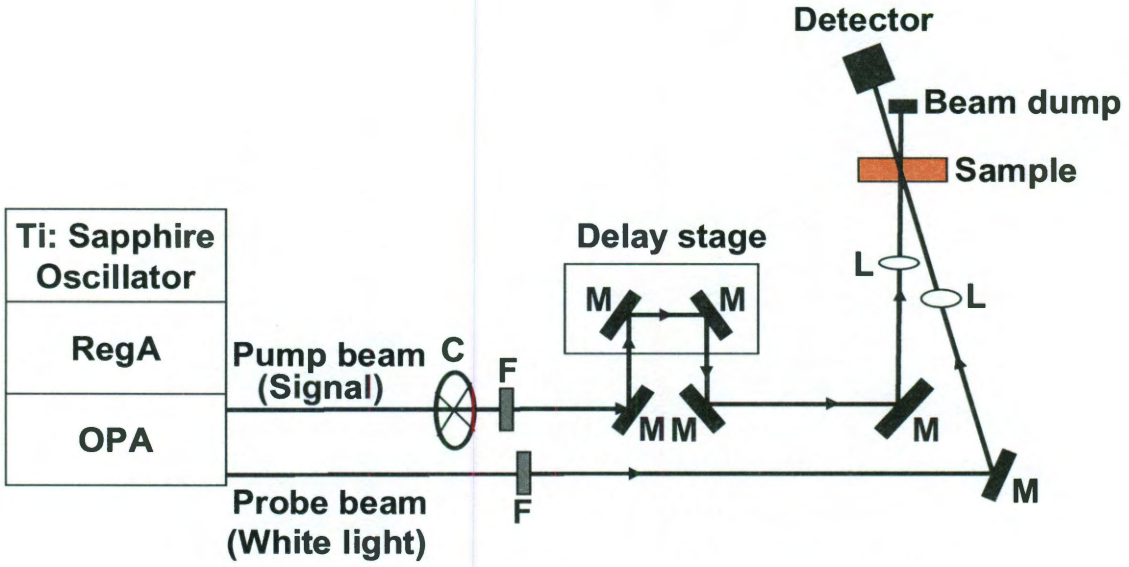

Fig.3.2: Schematic diagram of pump-probe experimental set-up. C: mechanical chopper, F: 10 nm bandpass filter, M: mirror, L: lens.

The ultrafast studies were performed using two-color, time-resolved pump-probe spectroscopy. A mode locked Ti:Sapphire laser system consisting of an oscillator (Coherent MIRA 900), a regenerative amplifier and an OPA (Coherent) was used as the excitation and probe source. Pulses from the OPA were approximately 150 fs. A motorized stage (Newport) was used to delay the probe beam with respect to the pump beam. The sample consisted of an aqueous solution of J-aggregate-Au nanoshell complexes in a 1 mm path length cuvette. Signals were collected in a transmission geometry.

3.4. Results: Time-Resolved Transmission Measurements

In Figure 3.3, the time-resolved transmission signals obtained from J-aggregate-Au nanoshell complexes (Fig. 3.3(a-d) are compared with those of J-aggregates in the absence of Au nanoshells (Fig. 3.3(e-h)). The pump and probe fluences are 60 $\mu J/cm^2$ and 0.8 $\mu J/cm^2$, respectively. This pump fluence is low enough such that no time-resolved signals were obtainable from nanoshells without J-aggregates under identical pump and probe conditions; in other words, only the transient dynamics of the J-aggregate and the J- aggregate complex are being probed. The FWHM of the laser spectrum was limited to 10 nm using a 10 nm band pass filter. The time-resolved relaxation dynamics shown in Figure 3.3 were obtained with pump and probe pulses at the same wavelength, for several discrete wavelengths within the spectral region of interaction, i.e., the Fano dip. These wavelengths (680 nm, 690 nm, 700 nm and 710 nm) are indicated in the nanoshell-J-aggregate extinction spectrum shown in Fig. 3.1(c).

For the J-aggregate-Au nanoshell complex, a clear transition from transient bleaching (pump and probe at 690 nm) to transient absorption (pump and probe at 710 nm) is observed, while no such transition can be observed for the pristine J-aggregate (Fig. 3.3(f-h)). The signal at 700 nm shows a complex, mixed transient bleaching and absorption behavior with the bleaching occurring at earlier times. At 680 nm, while the J-aggregate displays transient absorption (Fig. 3.3(e)),[92] the J-aggregate-Au nanoshell complex shows transient bleaching (Fig. 3.3(a)). The stark difference between the behavior of the plexcitonic complex and the pristine excitonic medium indicates a strong modification of the

excitonic states of the J-aggregate due to coupling with the localized dipolar plasmons of the Au nanoshells.[29]

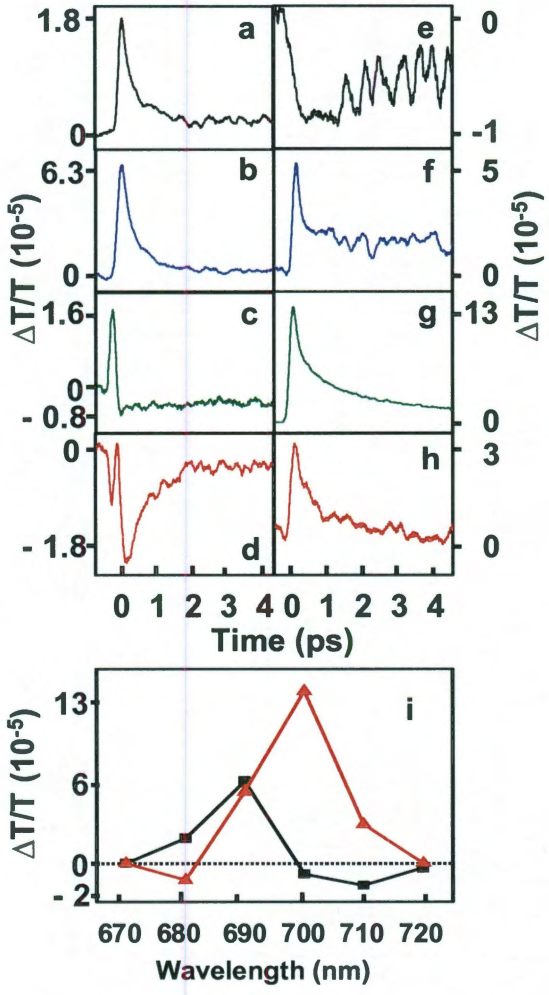

Figure 3.3: (a-d) Time-resolved differential transmission of J-aggregate-Au nanoshell complexes (corresponding extinction spectrum shown in Figure 1c). (e-h) Time-resolved differential transmission of pristine J-aggregates (corresponding extinction spectrum shown in Figure 1b). (a) and (e): pump and probe at 680 nm. (b) and (f): pump and probe at 690 nm. (c) and (g): pump and probe at 700 nm. (d) and (h): pump and probe at 710 nm. Pulse width of both pump and probe is 150 fs and pump fluence is approximately 60 μJ /cm^2. Fig. 2 (i): amplitude plots for J -aggregates (red triangles) and J-aggregate-nanoshell complexes (black squares).

We can explain the qualitative behavior of the transient signal in the vicinity of the Fano dip by considering both the nonlinear photo-bleaching of the J-aggregate and the Fano effect. When the plexcitonic system is excited by the pump pulse, the optical transition becomes partially saturated. From this we can infer that the Fano dip itself should become transiently modulated (a transient increase in intensity within the minimum of the Fano lineshape). This is due to the decreased exciton-plasmon interaction directly following excitation by the pump pulse. This transient increase within the Fano dip means an increase in transient absorption (and a corresponding decrease in transmission). This behavior should be limited to excitations within the Fano resonance: since strong exciton-plasmon coupling is not essential for the nonresonant optical response of the J-aggregates: outside the Fano resonance one would expect the usual transient bleaching of the excitonic system to be observed. The above effects (a negative ΔT at the Fano dip and a positive ΔT on the left-hand side of the Fano minimum) should create a shift of the Fano dip in the non-equilibrium absorption spectrum in the presence of optical pumping. Indeed, this transient shift can clearly be seen by comparing the experimental change in transmission $\Delta T/T$ as a function of wavelength for the plexcitonic complex and the J-aggregate shown in Fig. 3.3i. This figure also shows a decrease in magnitude of $\Delta T/T$ for the hybrid relative to the pristine J-aggregate (Fig. 3.3i). A plasmon resonance can, in principle, enhance the optical nonlinear response of a directly adjacent nonlinear material (in this case the J-aggregates) due to its high-intensity local electromagnetic field. However, in this case the presence of the metallic

component simultaneously leads to a faster relaxation of the nonequilibrium exciton population, which is the likely origin of the decrease in amplitude of $\Delta T/T$ observed (Fig. 3.3i).

3.5.1. Theoretical Nonlinear Model

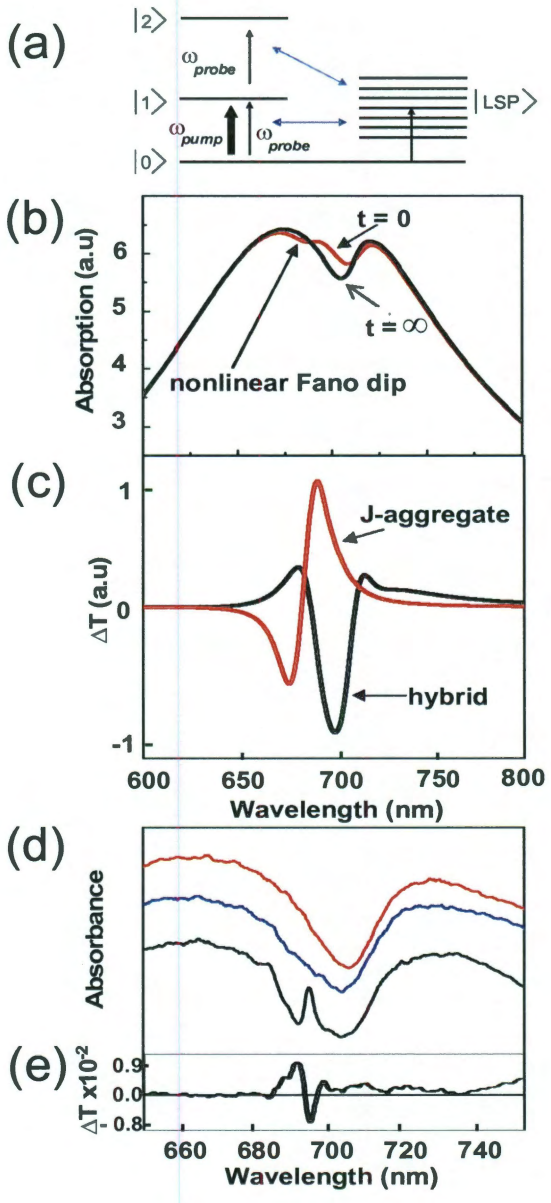

Figure 3.4: (a) Energy structure and transitions in a theoretical model describing the nonlinear Fano effect in our system. Vertical arrows (black) show optical transitions and the horizontal arrows (blue) depict exciton-plasmon coupling. (b) Calculated absorption of the J-aggregate-Au nanoshell complex at two times: t = 0 (pump-probe overlap) and t = ∞ (long-term equilibrium response). The nanoshell dimensions are $[r_1, r_2]$ = [48, 58] nm with a 2 nm thick J-aggregate shell layer. Parameters for the dielectric constants of the materials are taken from Ref. 28. (c) Normalized transient transmission at t = 0 for the hybrid complex (black) and for the pristine J-aggregates (red). (d) Experimental pump-continuum probe absorbance spectra of the J-aggregate-Au nanoshell complex pumped at 690 nm at various delay times: t = 0 overlap between pump pulse and continuum probe beam [black]; 80 ps delay [blue]. Continuum spectrum with no pump pulse present (beam blocked) [red]. Spectra displaced vertically for clarity. (e) Transient transmission obtained from excited state absorbance spectra shown in (d) by continuum background subtraction.

A straightforward theoretical model can be introduced that describes the observed plasmon-exciton coupling in the J-aggregate-Au nanoshell complex. Figure 3.4a shows the energy structure and transitions in our model.

The Fano interference appears in this model from the possibility for the photons to create a plasmon via two paths. In the resonance with the one-exciton, the paths are: $|0\rangle \rightarrow |LSP\rangle$ and $|0\rangle \rightarrow |1\rangle \rightarrow |LSP\rangle$. In the resonance with the two-exciton: $|1\rangle \rightarrow |LSP\rangle$ and $|1\rangle \rightarrow |2\rangle \rightarrow |LSP\rangle$. Photoinduced transmission in molecules alone is the universal behavior originating from saturation of a two-level (excitonic) system, consistent with the behavior of the pristine J-aggregate. Introducing the plasmon-exciton interaction requires that we extend this initial theoretical picture of the J-aggregate beyond a simple two-level system. We begin with a description of the exciton dynamics using rate equations that describe the populations of ground, one-exciton, and two-exciton states, $n_0(t)$, $n_{S1}(t)$ and $n_{S2}(t)$, that obey the condition: $n_0(t) + n_{S1}(t) + n_{S2}(t) = 1$. At

$-\delta t_{pulse} < t < 0$, a short pump pulse of duration δt_{pulse} excites both one-exciton and two-exciton states which rapidly relax. In our J-aggregates, these one-exciton and two-exciton states correspond to the states observed at the energies corresponding to ~700 and 680 nm, respectively. The two-exciton state can only be excited via the one-exciton state: for the pump intensities considered, $n_{S2}(t) < n_{S1}(t)$. To calculate the temporal evolution of the populations, we use a system of coupled rate equations and assume that the frequency of the pump beam is close to the Fano-dip spectral position ($\lambda = 700nm$). We then calculate the transient absorption of this system as a function of probe delay:

$$Q_{probe}(t) = \frac{1}{2}\mathrm{Re}\int_V \vec{j}^{*}(\vec{r},t)\cdot\vec{E}_{probe}(\vec{r})\,dV \quad , \qquad (1)$$

where $\vec{j}$ is the current inside the J-aggregate-Au nanoshell complex induced by a short, low-power probe pulse and $\vec{E}_{probe}$ is the nonuniform electric field inside the nanocomplex. The current is calculated as $\vec{j}(\vec{r},t) = -i\omega_{probe}\left(\varepsilon(\vec{r},t)-1\right)/4\pi\cdot\vec{E}_{probe}$, where $\varepsilon(\vec{r},t)$ is the effective dielectric constant of the system.[29] Inside the Au nanosphere, $\varepsilon(\vec{r},t) = \varepsilon_{Au}$, and inside the J-aggregate shell layer of the complex, $\varepsilon(\vec{r},t) = \varepsilon_J(t)$. The Au dielectric constant (ε_{Au}) remains a constant in this picture since, in this experimental regime, the nonlinearity of the Au subsystem is negligible (not observable at the fluences used). The nonlinear response enters this simple model via the time-dependent dielectric constant of the J-aggregate $\varepsilon_J(t)$ which can be described as:

$$\varepsilon_J(\omega,t) = 1 - f_{S1}\frac{\omega_{S1}^2}{\omega_{S1}^2 - \omega^2 + i\gamma\omega}\left(n_{S0}(t) - n_{S1}(t)\right) - f_{S2}\frac{\omega_{S2}^2}{\omega_{S2}^2 - \omega^2 + i\gamma\omega}\left(n_{S1}(t) - n_{S2}(t)\right),$$

(2)

where $f_{S1} = 0.03$ and $f_{S2} = 0.05$ are the reduced oscillator strengths, and $\gamma = 0.052eV$. These material parameters were obtained from the available literature on the J-aggregate system.[56, 92] The coefficients involving the nonequilibrium state populations in Eq. 2 describe the usual effect of bleaching of a molecular system.

Calculation of the electric current and the actual electric field inside the complex is relatively simple for a small nanocomplex in the quasistatic regime that applies here, i.e. when $c << \lambda$, where c and λ are the radius of the complex (c=60 nm) and the wavelength of probe light (λ= 680-710 nm), respectively. In this case, one can use the Poisson equation and obtain a result analytically.[56] Figure 3.4. shows the calculated absorption Q_{probe} at the beginning of the probe pulse ($t = 0$) and at long delay times ($t = \infty$) when the system comes to equilibrium. The transient transmission signal at t = 0 is $\Delta T_{\max} \propto Q_{probe}(t = \infty) - Q_{probe}(t = 0)$ and is shown in Figure 3.4(c). In Figure 3.4c, we see the formation of transient absorption (negative $\Delta T_{\max}$) in the spectral region of the Fano dip, as already discussed. Another predicted result from this model is the creation of a second, transient Fano dip in the vicinity of the linear Fano dip (Fig. 3.4b) due to

involvement of the two-exciton states (the transition $|1\rangle \rightarrow |2\rangle$ in the energy diagram of Fig. 3.4a). Compared to the nonlinear Fano model used in previous publications,[43, 93] a novel feature of the present model is the inclusion of the two-exciton states that adds a second nonlinear Fano minimum. This theoretical model is meant to provide a qualitative picture of the coupled system: detailed properties of the excitonic states, their various relaxation channels, and other effects such as spectral hole-burning are not described quantitatively by this simple picture.

3.5.2. Experimental Verification of Theory

Probing this coupled system experimentally with a short pump pulse and a continuum probe pulse whose spectral content spans the plexciton Fano resonance allows us to experimentally verify the theoretical predictions of our simple model (Fig. 3.4(d)). For the case of overlapping pump and probe pulses (t = 0), we are able to observe a significant modulation within the Fano dip. This additional spectral feature follows the modulation predicted from our theoretical model remarkably well (Fig. 3.4(c)). Here the pump pulse partially saturates the one-exciton transition in the complex. When this occurs we would anticipate that the depth of the Fano minimum would decrease with a transient absorption appearing within the spectral region of the Fano dip. Simultaneously, we would anticipate transient bleaching signals on the sides of this transient absorption region. These modulations are clearly observed (Fig. 3.4(e)). Interestingly, the above results mean that, with the pump pulse, we are able to modulate

selectively the strength of exciton-plasmon couplings in the spectrum. The pump pulse diminishes the one-exciton-plasmon coupling (negative ΔT for the dip region in Figs. 3.3i and 3.4e) and, simultaneously, activates the two-exciton-plasmon interaction (positive ΔT to the red from the Fano dip in Fig. 3.4e).

3.6. Conclusions

In conclusion, we have studied the ultrafast optical dynamics of excitons in nanoshell-J-aggregate complexes where localized plasmons and excitons are interacting strongly. The ultrafast characteristics indicate that these hybrid nanostructures might possess enhanced, tunable, on- and off- resonance nonlinear optical properties. We believe that these results may stimulate further interest in the properties of nanoengineered plasmon-exciton systems that may ultimately serve as active media in new classes of nonlinear optical devices or in active, functional metamaterials.

Chapter 4

Ultrafast all-Optical Modulation based on Strong Plasmon-Exciton Coupling

4.1. Introduction

Active plasmonic devices would usher in a new era of computation by making all-optical computing a reality. These devices would function as optical switches,[28] modulators,[94] amplifiers[3] and transistors[95] in all–optical integrated circuits. So far, the principles of operation for active plasmonic devices have been based on a shift of plasmon resonance due to change in refractive index of surrounding medium,[96] plasmon induced absorption in quantum dots,[94] plasmon attenuation using photochromic molecules[97] or increase in plasmon decay length due to change in refractive index of material sustaining the plasmons.[19] All these studies exploit properties of propagating plasmons. Loacalized plasmons, on the other hand, have a more intense near field than propagating plasmons. Recent studies have shown that placing excitonic nanostructures within these intense localized electromagnetic fields result to strong plasmon-exciton coupling.[13, 27, 29, 35] Active devices operating on the principle of plasmon-exciton coupling have not yet been explored.[87] This kind of coupling results to formation of hybridized states consisting of a mix of plasmons and excitons[22] and also Fano interference effects.[35] As a result of this coupling the plasmon-exciton system becomes transparent at the wavelength where plasmon and exciton energies are degenerate. The degree of transparency depends on the strength of coupling.

The ability of controlling this coupling strength thus gives rise to the possibility of using plasmon-exciton systems for modulation and switching applications. Devices that make use of strong plasmon-exciton interaction would be very sensitive, as such, consume very low power. They would also operate at very high speeds since plasmons have a very short life time. In order to build very compact all-optical integrated circuits with hundreds of functions, the individual components must have sub 100 nm dimensions. Strong plasmon-exciton coupling effect has been observed at single metallic nanoparticle level.[38] Using this coupling effect would be more advantageous than using Kerr nonlinearity of a single metallic nanoparticle since it is weak and requires high pump powers.[98]

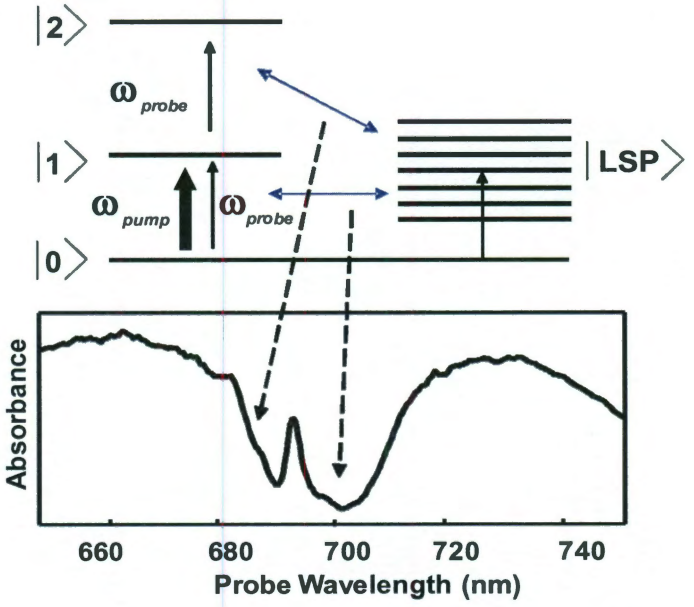

Fig. 4.1. Schematic energy level diagram of coupled plasmons and excitons, together with the extinction spectrum showing simultaneous coupling of both one- and two-excitons to plasmons. The plexcitonic system is pumped at 690 nm a probed with a white light continuum. The delay time between pump and probe pulses is 150 fs.

It has been shown in the previous chapter that the coupling energy between plasmons and excitons can be modulated at an ultrafast scale. The previous chapter also demonstrates that both one-excitons and two-excitons of J-aggregates can simultaneously couple strongly to plasmons as shown in Fig. 4.1 above. Here, we study the modulation properties of plexcitonic nanoparticles (gold nanoshell/J-aggreagte hybrids) based on simultaneous strong coupling of one and two- excitons to plasmons. We modulate the system by exciting a fraction of electrons from J-aggregate ground state to the J-aggregate one-exciton band at a specific pump wavelength and then observe the modulation effect by collecting transient dynamics signals at different probe wavelengths across the strong coupling regime (see appendices A1, A2, A3, and A4).

Plexcitonic nanoparticles are gold nanoshells coated with a thin layer of J-aggregates (see chapter 2, section 2.2). Gold nanoshells are plasmonic nanostructures that consist of a silica core and a gold shell (see chapter 1, section 1.4). J-aggregates on the other hand possess excitons with high oscillator strengths thus enabling them to couple strongly to localized surface plasmons of the gold nanoshell (see chapter 1, section 1.2). This study makes use of both the one-excitons and the two-excitons.[92] These excitons possess different resonant energies, so, they couple strongly to different plasmon wavelengths as shown in Fig. 4.1. Coupling of one-excitons to localized plasmons is linear while coupling of two-excitons to localized plasmons is nonlinear. This nonlinearity comes from the fact that the two-excitons can not be excited directly from the ground state.[92] Modulation is achieved by exerting

control over excited state carrier densities given that plasmon-exciton coupling strength is directly related to these carrier densities. Even though our study is based on ensemble measurements, it proves without doubt that ultrafast all-optical modulation can be implemented on a single metallic nanoparticle with sub 100 nm dimensions when coated with J-aggregate molecules.[38]

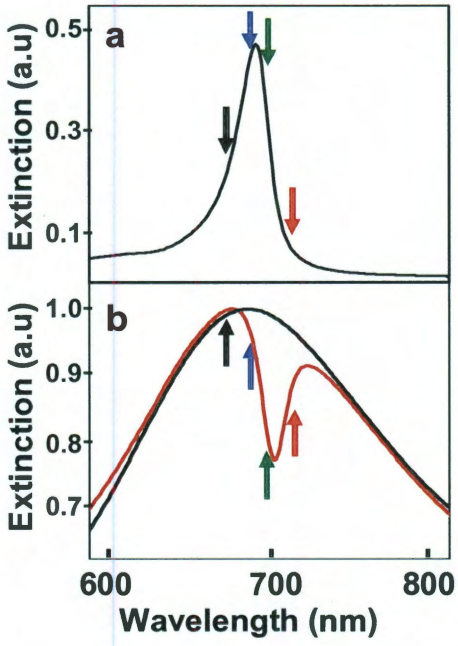

Fig. 4.2: Absorption of J-aggregates (a) and extinction spectra of nanoshells (black(b)) and plexcitonic nanoparticles (red (b)) with arrows indicating wavelengths where the system is optically modulated by pump pulse. Plexcitonic nanoparticles are modulated across the bandwidth where plasmons and excitons interact strongly.

The J-aggregates are formed on the surface of nanoshells when a water/ethanol (50:50) solution of dye molecules is added to an aqueous solution of nanoshells. A coherent coupling strength of 120 meV has been measured for plexcitonic nanoparticles.[29] The linear absorption spectrum of J-aggregates (Figure 4.2a) indicates a resonant transition wavelength of 695 nm for one-

excitons. The gold nanoshells used for this study have a resonance dipole plasmon wavelength of 690 nm (Figure 4.2b, black). Strong coupling between plasmons and one-excitons results to an increase in transparency of the plexcitonic nanoparticle at 700 nm (Figure 4.2b, red).

4.2. Ultrafast Modulation Properties of Plexcitonic Nanoparticles

In order to study the optical modulation properties of plexcitonic nanoparticles, I used the pump-probe technique (see chapter 3, section 3.3). The pump pulse modulates the system while the probe pulse detects the modulation effect. A mode locked Ti:Sapphire laser system that consists of an oscillator (MIRA 900), amplifier (RegA 9000) and an optical parametric amplifier (OPA 9400) from Coherent was used. The OPA produces 150 fs pulses at a rep. rate of 250 kHz.

As shown in Fig 4.2, 700 nm corresponds to minimum in extinction spectrum of plexcitonic nanoparticles. At this minimum, excitons interact destructively with the plasmon continuum implying that interaction between one-excitons and plasmons is strongest at 700 nm. We pump at the minimum (700 nm) (Figure. A3), and also, to the left (680 nm and 690 nm) (Figure A1 and Figure A2) and right (710 nm) (Figure A4) of the minimum. The pumped system is probed at discrete wavelengths between 660 nm and 730 nm (see appendices A1 to A4). The pump power is low enough that no transient nonlinearities are generated in the pristine gold nanoshells. Modulation effects become apparent by comparing signals from plexcitonic nanoparticles with signals from pure J-

aggregates (see appendices A1, A2, A3, and A4). There are two sources for the modulation effects. The first is a reduction in coupling strength between one-excitons and plasmons that result to a blue shift in the Fano minimum[99] and hence transient absorption at low energy. The second is coupling between two-excitons and plasmons resulting to a second Fano minimum at higher energies that give rise to transient bleaching. Modulation effects differ based on where the system is pumped. For example, the signal collected by probing at 700 nm changes as we tune the pump wavelength from 680 nm to 710 nm as shown in Fig. 4.3. When pumped at 680 nm and 690 nm, the probe signal at 700 nm shows transient absorption and when pumped at 700 nm, it is a mixture of transient bleaching and transient absorption. Meanwhile, when pumped at 710 nm, probe signal at 700 nm is transient bleach signal. The pump pulse creates excited state excitons (one-excitons) and the modulation effect at 700 nm is directly associated to the energy distribution of these one-excitons. **Note:** There are different one-exciton states within the one-exciton band[31-33, 100] of the J-aggregate and the states occupied after excitation by pump pulse depends on the pump pulse energy. This is illustrated by arrows indicating the respective pump wavelengths on the linear absorption spectrum of J-aggregate in Figure 4.2a. Creation of one-excitons leads to decrease in ground state exciton population which results to decrease in coupling strength between one-excitons and plasmons. Also, excitation of one-excitons implies the channel for excitation of two-excitons becomes open. As such, plasmons also couple strongly to two-

excitons at wavelengths to the blue of the one-exciton transition wavelength as shown in Fig. 4.1.

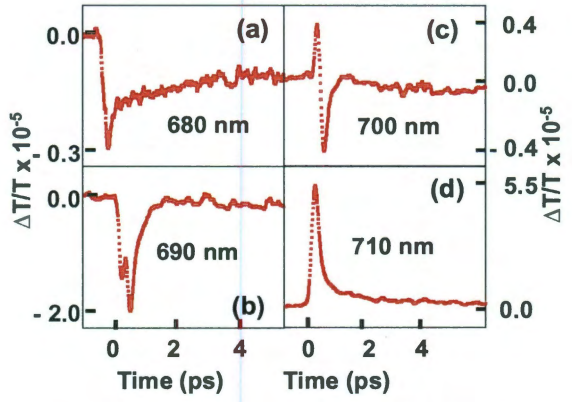

Fig. 4.3: Modulation properties of plexcitonic nanoparticles. Transient transmission signals change sign when plexcitonic nanoparticle are probed at 700 nm and pumped at discrete wavelengths from 680 nm to 710 nm.

Generally, modulation by pump beam (680 nm, 690 nm, 700 nm or 710 nm) simultaneously initiates strong coupling between two-excitons and plasmons and decreases strong coupling between one-excitons and plasmons. When pumped at 680 nm and 690 nm, the one-exciton dipole moment at 700 nm is greatly reduced, as such, coupling strength decreases leading to observation of transient absorption. Pumping at 700 nm causes the two modulation effects (decrease in coupling strength between one-exciton and plasmons, and, increase in coupling strength between two-excitons and plasmons) to appear simultaneously at 700 nm. It is important to note that there are different two-exciton states within the J-aggregate two-exciton band.[31-33, 100] Pumping at 700 nm leads to generation of two-excitons with energies close to 700 nm (see Fig. A3 in appendix). This implies that the energy separation between modulation

effects when pumped at 700 nm tends to be very small. Also, note that the FWHM of the pump pulse is between 5 and 10 nm. In the signal shown in Fig. 4.3c, transient bleaching appears before transient absorption. This may be because the probe pulse is more sensitive to coupling of two-excitons to plasmons due to the nonlinear nature of the coupling. A very small fraction of probe energy saturates the transition from one-exciton state to two-exciton state while the remainder of the energy goes to excite the plasmon continuum. As such, interference between the plasmon continuum and exciton state becomes stronger making it more sensitive to probe beam. Pumping at 710 nm does not affect the one- exciton dipole moment at 700 nm. Hence, the dominant modulation effect at 700 nm when pumped at 710 nm is two-exciton coupling which leads to transient bleaching.

Another modulation feature due to strong coupling is the blockade of electron flow from one-exciton band to gold conduction band. That is, after pump pulse excites excitons to the one-exciton band, the electrons associated to these excitons do not flow over to the conduction band of gold as reported for the case when plasmon and excitons couple weakly.[56] This is obvious from the extremely fast relaxation of excitons to the J-aggregate ground state in the plexcitonic nanoparticle. Electron flow from one-exciton band to gold conduction band and back to J-aggregate ground state would certainly take longer than the 2 ps relaxation time observed in our measurements (Fig. 4.4). The 2 ps relaxation time is approximately equal to electron-phonon decay time in gold nanoshell.[101]

This supports the fact that energy flows from one-excitons to plasmons through the Forster energy process.

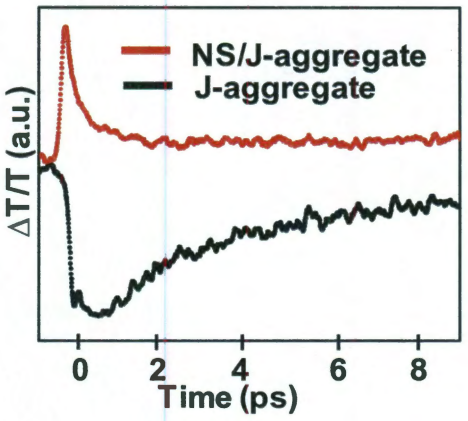

Fig. 4.4: Transient signal from plexcitonic nanoparticles obtained by pumping and probing at 680 nm. Transient bleached signal is obtained as opposed to transient absorption from pristine J-aggregates pumped and probed under identical conditions. Carriers relax in less than 2 ps indicating that there is no charge transfer from J-aggregate to gold nanoshell.

The decay time of transient absorption signals from plexcitonic nanoparticles show no power dependence. Fig. 4.5b shows transient signals from plexcitonic nanoparticles pumped at 700 nm and probed at 710 nm with pump powers of 50 μW (black) and 2.5 mW (red). The probe power is kept fixed at 1.5 μW. An increase in pump power by a factor of 50 does not lead to any changes in decay dynamics within plexcitonic nanoparticles. This is in sharp contrast to the case of pristine J-aggregates (Fig. 4.5a) where increase in pump power gives rise to exciton-exciton annihilation.[34] This is an interesting difference

between plexcitons (plasmon-exciton hybrids) and excitons. It indicates that strong coupling of excitons to plasmons dominates or shunts the exciton-exciton annihilation process.

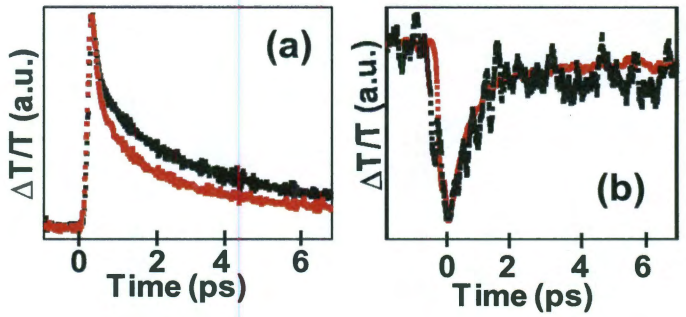

Fig. 4.5: Transients signals from (a): Pristine J-aggregates pumped and probed at 700 nm. Pump power is 200 μW (black) and 1 mW (red), while probe power is constant at 4 μW. (b): Plexcitonic nanoparticles pumped at 700 nm and probed at 710 nm. Pump power is 50 μW (black) and 2.5 mW (red) while probe power is 1.5 μW. Strong plasmon exciton coupling shunts or blocks exciton-exciton annihilation.

4.3. Conclusions

In conclusion, I have studied the ultrafast all-optical modulation properties of plexcitonic nanoparticles. Based on these properties, it is possible to design and fabricate active plasmonic devices which function on the principle of strong plasmon-exciton coupling. Furthermore, the ability to tune plasmon resonant wavelength of gold nanoshells makes it possible for plexcitonic nanoparticles to function at optical communication wavelengths.[102] This is because J-aggregates

have been synthesized with exciton resonance at the optical communication wavelength. The use of excited state excitons of J-aggregates to achieve active control can be extended to other exciton systems like quantum dots. Our studies open the way for achieving active control at the single metallic nanoparticle level.

Chapter 5

Conclusions

This thesis covers basics of the linear and nonlinear optical properties of strongly coupled plasmon/exciton hybrid nanostructures. The very simple hybrid structure consisting of gold nanoshell coated with J-aggregates used in this work presents a unique platform for further in-depth studies of fundamental physics of coupled plasmon/exciton nano-systems. The gold nanoshell/J-aggregates hybrid sustains two different types of nonlinear Fano effect. The first is nonlinear Fano due to coupling of two-excitons of J-aggregates to gold nanoshell plasmons, as shown in this thesis. The second type of nonlinear Fano effect is associated to saturation of one-exciton transition.[43, 93] This has been theoretically predicted for a quantum_dot/gold_nanoparticle hybrid[43] and experimentally observed for a quantum dot coupled to a 2-D electron gas.[93] A possible future direction based on the work in this thesis could be to investigate the differences between these two nonlinear Fano effects given that they are sustained by the same hybrid structure.

Another possibility stemming from this work would be to study how exciton-exciton annihilation is influenced by plasmon/exciton coupling. This thesis provides initial evidence suggesting that exciton-exciton annihilation is absent in the presence of strong plasmon/exciton coupling. Further experimental and theoretical work is necessary to fully understand the impact that plasmon/exciton coupling has on exciton-exciton annihilation.

With proper modification of the plasmon/exciton hybrid system, it will be possible to study the transition from Fano interference to the regime of vacuum Rabi splitting. The plasmon-exciton coupling strength is higher in the vacuum Rabi splitting regime than it is in the Fano interference regime. With an appropriate plasmonic structure, for example dimer nano-gaps, it will be possible to achieve vacuum Rabi splitting in a plasmon-exciton hybrid.[7] This is because the short lifetime of plasmons will be compensated by the high photon density of plasmons. As experimentally demonstrated in this thesis and also in the work of Vasa et al,[87] pumping a plasmon/exciton hybrid structure with an ultrashort optical pulse leads to modulation of the plasmon/exciton coupling strength. As such, another future research direction could be the dynamic tuning of plasmon/exciton coupling strength that will ultimately lead to a transition from vacuum Rabi splitting (higher coupling strength) to regime of Fano interference (smaller coupling strength) on the same hybrid structure. This work encourages the study of such transition in the very near future.

A combination of the hybrid structure and nonlinear pump probe technique employed in this study opens up the possibility to study the influence that coupling of excitons to plasmons has on the transient response of gold nanoshells. This thesis is limited to the case where the pump pulse is not intense enough to induce transients in the gold nanoshell. Also, the simultaneous coupling of one-excitons and two-excitons to plasmons implies that plasmons can initiate mixing of one-excitons and two-excitons. It will be interesting to explore properties of mixed one- and two-excitons.

Another interesting area not explored in this thesis is the study of fluorescence from hybrid in the strong coupling regime. It will be important to observe if there is any kind of spectral modification[103] of the fluorescence given that strong coupling of excitons to plasmons can lead to shifting and splitting of exciton energy levels. Also, an experimental study of how changes in the dielectric environment[39] affect linear optical properties of J-aggregate were not addressed in this thesis. Such environmental dielectric changes result from tuning the gold nanoshell plasmon across the one-exciton absorption band of the J-aggregate. The simple gold nanoshell/J-aggregate hybrid together with its linear and nonlinear optical properties presented in this work makes such a study plausible and achievable.

References

1. Maier, S. A., *Plasmonics: Fundamentals and Applications*. Springer: 2007.
2. Stockman, M. I. *Physics Today* **February 2011**, page 39.
3. Stockman, M. I. *Journal of Optics* **2010,** 12, 024004-024016.
4. Lassiter;, J. B.; Aizpurua;, J.; Hernandez;, L. I.; Brandl;, D. W.; Romero;, I.; Lal;, S.; Hafner;, J. H.; Nordlander;, P.; Halas., N. J. *Nano Letters* **2008,** 8, (4), 1212-1218.
5. Talley;, C. E.; Jackson;, J. B.; Oubre;, C.; Grady;, N. K.; Hollars;, C. W.; Lane;, S. M.; Huser;, T. R.; Nordlander;, P.; Halas., N. J. *Nano Letters* **2005,** 5, (8), 1569-1574.
6. Xiaohua Wu; Stephen K. Gray; Pelton, M. *optics express* **2010,** 18, (23), 13.
7. Salvatore Savasta; Rosalba Saija; Alessandro Ridolfo; Omar Di Stefano; Paolo Denti; Borghese., F. *ACS Nano* **2010,** 4 (11), 6369-6376.
8. Sönnichsen, C.; Franzl, T.; Wilk, T.; Plessen, G. v.; Feldmann, J.; Wilson, O.; Mulvaney., P. *Physical Review Letters* **2002,** 88, 4.
9. Nehl, C. L.; Grady, N. K.; Goodrich, G. P.; Tam, F.; Halas, N. J.; Hafner., J. H. *Nano Letters* **2004,** 4, (12), 2355-2359.
10. Halas, N. J.; Lal, S.; Chang, W.-S.; Link, S.; Nordlander., P. *Chem. Rev.* **2011,** 111, 3913-3961.
11. Halas, N. J. *Nano letters* **2010,** 10, 3816-3822.
12. Oldenburg, S. J.; Averitt, R. D.; Westcott, S. L.; Halas, N. J. *Chem. Phys. Lett* **1998,** 288, 243 - 247.
13. Sugawara, Y.; Kelf, T. A.; Baumberg, J. J.; Abdelsalam, M. E.; Bartlett, P. N. *Phys. Rev. Lett.* **2006,** 97, 266808.
14. Larsson, E. M.; Alegret, J.; Kall, M.; Sutherland., D. S. *Nano letters* **2007,** 7, (5), 1256-1263.
15. Mukherjee;, S.; Sobhani;, H.; Lassiter;, J. B.; Bardhan;, R.; Nordlander;, P.; Halas., N. J. *Nano Letters* **2010,** 10, (7), 2694-2701.
16. Bardhan, R.; Lal, S.; Joshi, A.; Halas., N. J. *Acc. Chem. Res.* **2011**, DOI: 10.1021/ar200023x.
17. Jackson;, J. B.; Halas;, N. J.; Kinsey., J. L. *PNAS* **2004,** 101, (52), 17930-17935.
18. Atwater, H. A.; Polman., A. *Nature Materials* **2010,** 9, 205-213.
19. Kevin F. Macdonald; Zsolt L. Samson; Mark I. Stockman; Zheludev, N. I. *nature photonics* **2009,** 3, 55-58.
20. Hirsch, L. R.; Stafford, R. J.; Bankson, J. A.; Sershen, S. R.; Rivera, B.; Price, R. E.; Hazle, J. D.; Halas, N. J.; West, J. L. *PNAS* **2003,** 100, 13549-13554
21. Tam, F.; Moran, C.; Halas., N. J. *J. Phys. Chem. B* **2004,** 108, 17290-17294.
22. Ambjornsson, T.; Mukhopadhyay, G.; Apell, S. P.; Kall, M. *Phys. Rev. B* **2006,** 73, 085412
23. Oubre, C.; Nordlander., P. *J. Phys. Chem. B* **2005,** 109, 10042-10051.

24. Prodan, E.; Radloff, C.; Halas, N. J.; Nordlander, P. *Science* **2003,** 302, 419-422.
25. Shelton, D. J.; Brener, I.; Ginn, J. C.; Sinclair, M. B.; Peters, D. W.; Coffey, K. R.; Boreman., G. D. *Nano letters* **2011,** 11, (5), 2104–2108.
26. Diane Djoumessi Lekeufack; arnaud Brioude; Anthony W. coleman; Philippe Miele; Joel Bellessa; Li De Zeng; Stadelmann., P. *Applied Physics Letters* **2010,** 96, 253107-253109.
27. Wiederrecht, G. P.; Hall, J. E.; Bouhelier, A. *Phys. Rev. Lett.* **2007,** 98, 083001.
28. A. V. Krasavin; Zheludev, N. I. *Applied Physics Letters* **2004,** 84, (8), 1416-1418.
29. Fofang, N. T.; Park, T.; Neumann, O.; Mirin, N. A.; Nordlander, P.; Halas, N. J. *Nano Lett.* **2008,** 8, (10), 3481-3487.
30. Fofang;, N. T.; Grady;, N.; Fan;, Z.; Govorov;, A. O.; Halas., N. J. *nano letters* **2011,** 11, 1556-1560.
31. Kobayashi, T. *J-Aggregates by World Scientific Publishing* **1996**.
32. Spano, F. C.; Mukamel, S. *J. Chem. Phys* **1989,** 91, (2), 683-700.
33. Spano, F. C.; Mukamel, S. *Phys. Rev. A* **1989,** 40, (10), 5783-5801.
34. Gadonas, R. *J. Chem. Phys* **1997,** 106, (20), 8374-8383.
35. Kelley, A. M. *Nano Lett.* **2007,** 7, (10), 3235-3240.
36. Fano, U. *Phys. Rev.* **1961,** 124, 1866-1878.
37. Govorov, A. O.; Lee, J.; Kotov, N. A. *Phys. Rev. B* **2007,** 76, 125308.
38. Weihai Ni; Tobias Ambjornsson; Sten Peter Apell; Huanjun Chen; Wang, J. *nano letters* **2010,** 10, (1), 77-84.
39. Gulen, D. *J. Phys. Chem. C* **2010,** 114, 13825–13831.
40. Fan;, J. A.; Bao;, K.; Wu;, C.; Bao;, J.; Bardhan;, R.; Halas;, N. J.; Manoharan;, V. N.; Shvets;, G.; Nordlander;, P.; Capasso., F. *Nano Letters* **2010,** 10, (11), 4680-4685.
41. Luk'yanchuk;, B.; Zheludev;, N. I.; Maier;, S. A.; Halas;, N. J.; Nordlander;, P.; Giessen;, H.; Chong., C. T. *Nature Materials* **2010,** 9, (9), 707-715.
42. Fan, J. A.; Wu, C.; Bao, K.; Bao, J.; Bardhan, R.; Halas, N. J.; Manoharan, V. N.; Nordlander, P.; Shvets, G.; Capasso, F. *Science* **2010,** 328, 1135-1138.
43. Zhang, W.; Govorov, A. O.; Bryant, G. W. *Phys. Rev. Lett* **2006,** 97, 146804.
44. Oldenburg;, S. J.; Hale;, G. D.; Jackson;, J. B.; Halas., N. J. *Applied Physics Letters* **1999,** 75, (8), 1063-1065.
45. Prodan;, E.; Nordlander., P. *nano letters* **2003,** 3, 543-547.
46. Bishnoi, S. W.; Rozell, C.; Levin, C. S.; Gheith, M. K.; Johnson, B. R.; Johnson, D. H.; Halas, N. J. *Nano Lett.* **2006,** 6, 1687-1692.
47. Govorov, A. O.; Carmeli, I. *Nano Lett.* **2007,** 7, 620 - 625.
48. Slocik;, J. M.; Tam;, F.; Halas;, N. J.; Naik, R. R. *Nano Letters* **2007,** 7, 1054-1058.
49. Zhao, J.; Zhang, X.; Yonzon, C. R.; Haes, A. J.; Van Duyne, R. P. *Nanomedicine* **2006,** 1, 219-228.

50. Crespo;, P.; Litrán;, R.; Rojas;, T. C.; Multigner;, M.; Fuente;, J. M. d. l.; Sánchez-López;, J. C.; García;, M. A.; Hernando;, A.; Penadés;, S.; Fernández., A. *Physical review letters* **2004,** 93, 087204.
51. Tam, F.; Goodrich, G. P.; Johnson, B. R.; Halas, N. J. *Nano Lett.* **2007,** 7, 496 - 501.
52. Dulkeith, E.; Morteani, A. C.; Niedereichholz, T.; Klar, T. A.; Feldmann, J.; Levi, S. A.; Veggel, F. C. J. M. v.; Reinhoudt, D. N.; Mo¨ller, M.; Gittins, D. I. *Phys. Rev. Lett.* **2002,** 89, 203002.
53. Dintinger, J.; Klein, S.; Bustos, F.; Barnes, W. L.; Ebbessen, T. W. *Phys. Rev. B* **2005,** 71, 035424.
54. Bellessa, J.; Bonnand, C.; Plenet, J. C.; Mugnier, J. *Phys. Rev. Lett.* **2004,** 93, 036404.
55. Wurtz, G. A.; Evans, P. R.; Hendren, W.; Atkinson, R.; Dickson, W.; Pollard, R. J.; Zayats, A. V.; Harrison, W.; Bower, C. *Nano Lett.* **2007,** 7, 1297-1303.
56. Wiederrecht, G. P.; Wurtz, G. A.; Hranisavljevic, J. *Nano Lett.* **2004,** 4, 2121 - 2125.
57. Prodan;, E.; Nordlander., P. *J. Chem. Phys.* **2004,** 120, (11), 5444-5454.
58. Song, J.; He, Y.; Nurmikko, A. V.; Tischler, J.; Bulovic, V. *Phys. Rev. B* **2004,** 69, 235330
59. Hobson, P. A.; Barnesa, W. L.; Lidzey, D. G.; Gehring, G. A.; Whittaker, D. M.; Skolnick, M. S.; Walker, S. *Appl. Phys. Lett.* **2002,** 81, (4), 3519 -.
60. Lidzey, D. G.; Bradley, D. D. C.; Armitage, A.; Walker, S.; Skolnick, M. S. *Science* **2000,** 288 1620
61. Lidzey, D.; Bradley, D.; Skolnick, M.; Virgili, E.; Walker, S. *Phys. Rev. Lett.* **1999,** 82, 3316

62. Laboratories., H. B.
63. Jain;, P. K.; Eustis;, S.; El-Sayed., M. A. *J. Phys. Chem. B* **2006,** 110, 18243-18253.
64. Johnson, P. B.; Christy, R. W. *Phys. Rev. B* **1972,** 6, 4370 - 4379.
65. Bohren, C. F.; Huffmann, D. R., *Absorption and scattering of light by small particles*. John Wiley and sons: New York, 1998.
66. Scaife, B. K. P., *Principles of dielectrics*. Oxford science Publications: 1998.
67. Prodan;, E.; Lee;, A.; Nordlander., P. *Chem. Phys. Lett.* **2002,** 360, 325-332.
68. Min, C.; Wang, P.; Chen, C.; Deng, Y.; Lu, Y.; Ming, H.; Ning, T.; Zhou, Y.; Yang, G. *Optics Letters* **2008,** 33, (8), 869-871.
69. Dintinger, J.; Robel, I.; Kamat, P. V.; Genet, C.; Ebbesen, T. W. *Adv. Mater.* **2006,** 18, 1645 - 1648.
70. Dintinger, J.; Klein, S.; Ebbesen, T. W. *Adv. Mater.* **2006,** 18, 1267-1270.
71. Haraguchi, M.; Fukui, M.; Tamaki, Y.; Okamoto, T. *Journal of Microscopy* **2003,** 210, 229-233.
72. Sato, Y.; Furuki, M.; Minquan, T.; Iwasa, I.; Pu, L. S.; Tatsuura, S. *Appl. Phys. Lett* **2002,** 80, (13), 2254-2256.

73. Artuso, R. D.; Bryant, G. W. *Nano Lett* **2008,** 8, (7), 2106-2111.
74. Min, C.; Wang, P.; Chen, C.; Jiao, X.; Deng, Y.; Ming, H. *Optics Express* **2007,** 15, (19), 12368.
75. Wurtz, G. A.; Pollard, R.; Zayats, A. V. *Phys. Rev. Lett* **2006,** 97, 057402.
76. Porto, J. A.; Martin-Moreno, L.; Garcia-Vidal, F. J. *Phys. Rev. B* **2004,** 70, 081402.
77. Ispasoiu, R. G.; Balogh, L.; Varnavski, O. P.; Tomalia, D. A.; III, T. G. *J. Am. Chem. Soc* **2000,** 122, 11005-11006.
78. Dionne, J. A.; Diest, K.; Sweatlock, L. A.; Atwater, H. A. *Nano Lett* **2009,** 9, (2), 897-902.
79. Dicken, M. J.; Sweatlock, L. A.; Pacific, D.; Lezec, H. J.; Bhattacharya, K.; Atwater, H. A. *Nano Lett* **2008,** 8, (11), 4048-4052.
80. Wang, Y.; Xie, X.; III, T. G. *Nano Lett* **2005,** 5, (12), 2379-2384.
81. Lu, Z.; Zhu, K. *J. Phys. B: at. Mol. Opt. Phys.* **2008,** 41, 185503.
82. Kohlgraf-Owens, D. C.; Kik, P. G. *Optics Express* **2008,** 16, (14), 10823-10834.
83. Larkin, I. A.; Stockman, M. I.; Achermann, M.; Klimov, V. I. *Phys. Rev. B* **2004,** 69, 121403.
84. Felicia Tam; Allen L. Chen; Janardan Kundu; Hui Wang; Halas, N. J. *Journal of chemical physics* **2007,** 127, 6.
85. Lidzey, D. G.; Bradley, D. D. C.; Skolnick, M. S.; Virgili, T.; Walker, S.; Whittaker, D. M. *Nature* **1998,** 395, 53-55.
86. Sasaki, F.; Haraichi, S.; Kobayashi, S. *IEEE J. Quantum Electronics* **2002,** 38, (7), 943.
87. Vasa, P.; Pomraenke, R.; Cirmi, G.; Re, E. D.; Wang, W.; Schwieger, S.; Leipold, D.; Runge, E.; Cerullo, G.; Lienau, C. *ACS Nano* **2010,** 4, 7559-7565.
88. Hao;, F.; Nordlander;, P.; Sonnefraud;, Y.; Dorpe;, P. V.; Maier., S. A. *ACS Nano* **2009,** 3, (3), 643-652.
89. Verellen;, N.; Sonnefraud;, Y.; Sobhani;, H.; Hao;, F.; Moshchalkov;, V. V.; Dorpe;, P. V.; Nordlander;, P.; Maier., S. A. *Nano Letters* **2009,** 9, (4), 1663-1667.
90. Brown;, L. V.; Sobhani;, H.; Lassiter;, J. B.; Nordlander;, P.; Halas., N. J. *ACS Nano* **2010,** 4, (2), 819-832.
91. Sonnefraud;, Y.; Verellen;, N.; Sobhani;, H.; Vandenbosch;, G. A. E.; Moshchalkov;, V. V.; Dorpe;, P. V.; Nordlander;, P.; Maier., S. A. *ACS Nano* **2010,** 4, (3), 1664-1670.
92. Fidder, H.; Knoester, J.; Wiersma, D. *Journal of chemical physics* **1993,** 98, (8), 6564-6566.
93. M. Kroner; A. O. Govorov; S. Remi; B. Biedermann; S. Seidl; A. Badolato; P.M.Petroff; W. Zhang; R. Barbour; B. D. Gerardot; R. J. Warburton; Karrai, K. *Nature* **2008,** 451, 311-314.
94. Domenico Pacifici; Henri J. Lezec; Atwater., H. A. *nature photonics* **2007,** 1, 402-406.
95. Darrick E. Chang; Anders S. Sorensen; Eugene A. Demler; Lukin, M. D. *nature physics* **2007,** 3, 807-812.

96. Vincent K. S. Hsiao; Yue Bing Zheng; Bala Krishna Juluri; Huang, T. J. *advanced materials* **2008,** 20, 3528-3532.
97. Ragip A. Pala; Ken T. Shimizu; Nicholas a. Melosh; Brongersma, M. L. *nano letters* **2008,** 8, (5), 1506-1510.
98. Y. Hamanaka; A. Nakamura; S. Omi; N. Del Fatti; F. Vallee; Flytzanis, C. *Applied Physics Letters* **1999,** 75, (12), 1712-1714.
99. Manjavacas, A.; Abajo, F. J. G. d.; Nordlander, P. *nano letters* **2011,** 11, 2318–2323.
100. Fidder, H.; Knoester, J.; Wiersma, D. A. *J. Chem. Phys* **1993,** 98, (8), 6564-6566.
101. Averitt, R. D.; Westcott, S. L.; Halas, N. J. *J. Opt. Soc. Am. B* **1999,** 16, (10), 1814-1823.
102. Satoshi Tatsuura; Minquan Tian; Makoto Furuki; Yasuhiro Sato; Izumi Iwasa; Mitsu, H. *Applied Physics Letters* **2004,** 84, (9), 3.
103. Ringler, M.; Schwemer, A.; Wunderlich, M.; Nichtl, A.; Ku¨rzinger, K.; Klar, T. A.; Feldmann, J. *Physical review letters* **2008,** 100, 203002.

Appendix A1

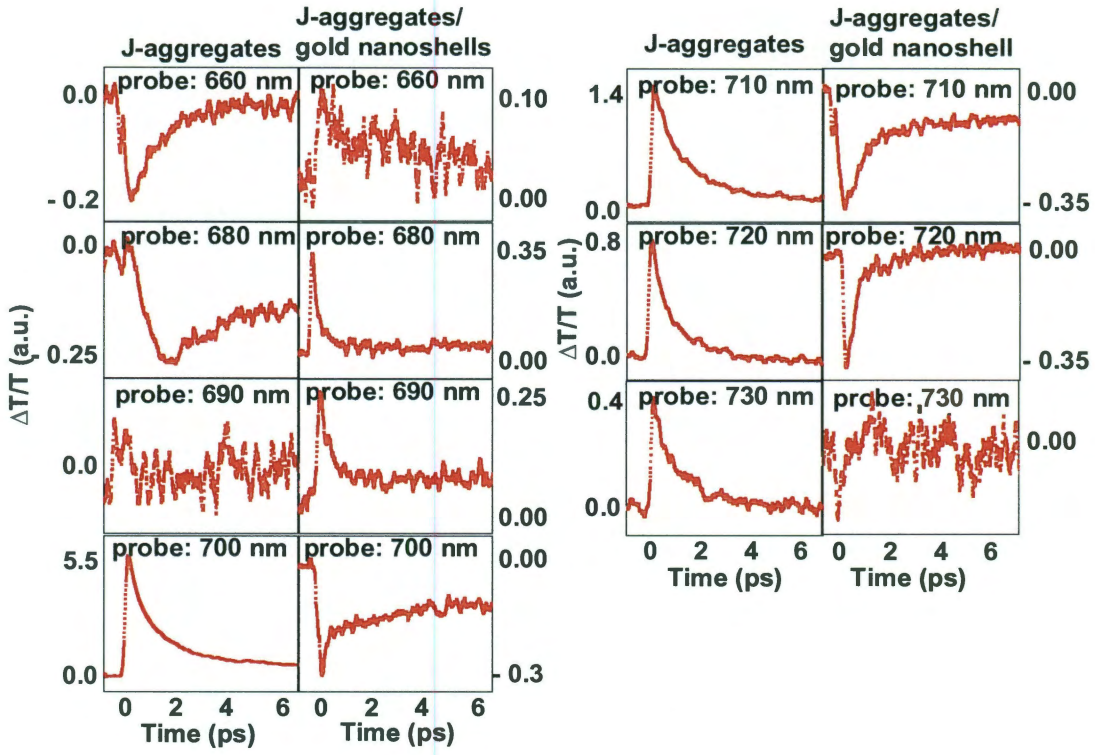

Fig. A1: Transient transmission signals obtained from J-Aggregates and J-Aggregate/Au-Nanoshell hybrid structures. The systems are pumped at 680 nm and probed at discrete wavelengths from 660 nm to 730 nm. Pump power is 200 μW and probe power is 4 μW. J-Aggregates show a transition from transient absorption to transient bleach at 690 nm, while, hybrid structures show a transition from transient bleach to transient absorption at 700 nm. Pump power is low enough that no transient signals are obtained from pristine Au-Nanoshells

Appendix A2

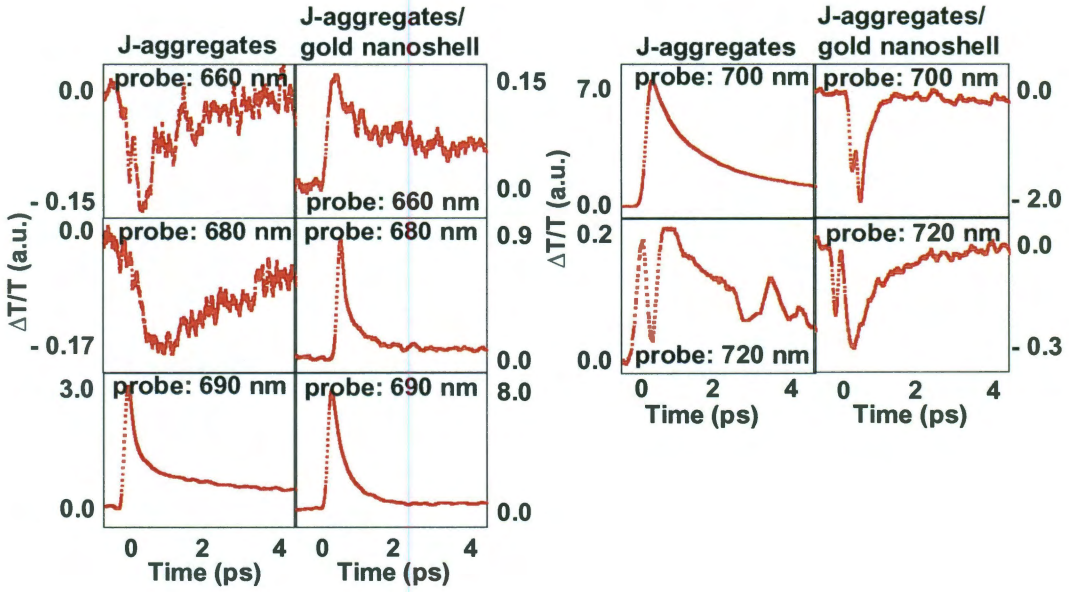

Fig. A2: Transient transmission signals obtained from J-Aggregates and J-Aggregate/Au-Nanoshell hybrid structures. The systems are pumped at 690 nm and probed at discrete wavelengths from 660 nm to 720 nm. Pump power is 200 μW and probe power is 4 μW. J-Aggregates show a transition from transient absorption to transient bleach at 690 nm, while, hybrid structures show a transition from transient bleach to transient absorption at 700 nm. Pump power is low enough that no transient signals are obtained from pristine Au-Nanoshells

Appendix A3

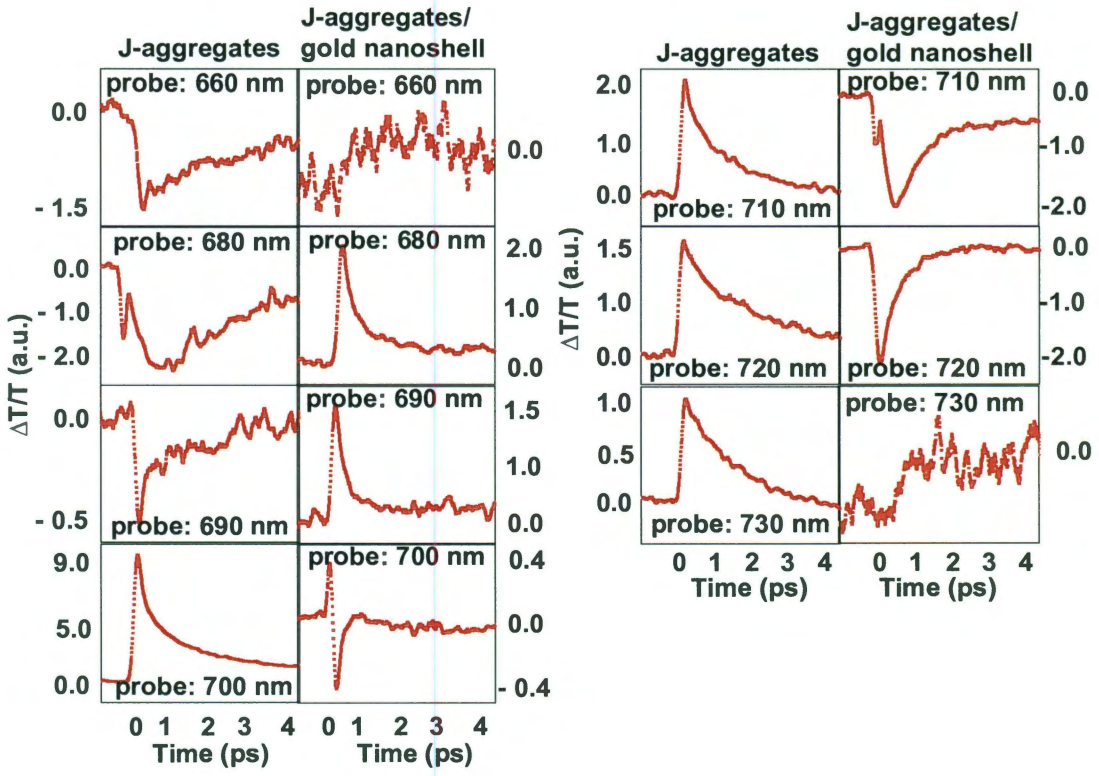

Fig. A3: Transient transmission signals obtained from J-Aggregates and J-Aggregate/Au-Nanoshell hybrid structures. The systems are pumped at 700 nm and probed at discrete wavelengths from 660 nm to 730 nm. Pump power is 200 μW and probe power is 4 μW. J-Aggregates show a transition from transient absorption to transient bleach at 700 nm, while, hybrid structures show a transition from transient bleach to transient absorption at 700 nm. Pump power is low enough that no transient signals are obtained from pristine Au-Nanoshells

Appendix A4

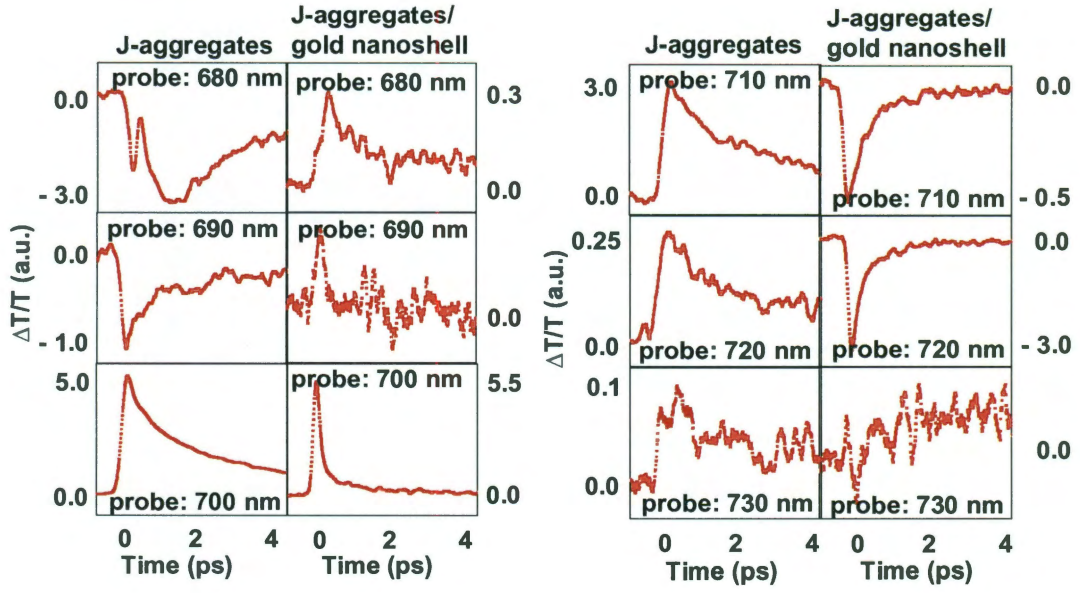

Fig. A4: Transient transmission signals obtained from J-Aggregates and J-Aggregate/Au-Nanoshell hybrid structures. The systems are pumped at 710 nm and probed at discrete wavelengths from 680 nm to 730 nm. Pump power is 200 μW and probe power is 4 μW. J-Aggregates show a transition from transient absorption to transient bleach at 700 nm, while, hybrid structures show a transition from transient bleach to transient absorption at 710 nm. Pump power is low enough that no transient signals are obtained from pristine Au-Nanoshells